Average charged-particle multiplicities in $\pi^- p$ inclusive reactions at 147 GeV/c

D. Brick, D. Fong,* M. Heller,† A. M. Shapiro, and M. Widgoff
Brown University, Providence, Rhode Island 02912

F. Bruyant
CERN, Geneva 23, Switzerland

D. Bogert and M. Johnson
Fermilab, Batavia, Illinois 60510

R. Burnstein, C. Fu,‡ D. Petersen,§ M. Robertson,‖ and H. Rubin
Illinois Institute of Technology, Chicogo, Illinois 60616

R. D. Sard, A. Snyder,¶ and J. Tortora**
University of Illinois, Urbana, Illinois 61801

E. D. Alyea, Jr.
Indiana University, Bloomington, Indiana 47401

C.-Y. Chien, P. Lucas,†† A. Pevsner, and R. Zdanis
John Hopkins University, Baltimore, Maryland 21218

F. Barreiro, O. Benary,‡‡ J. E. Brau,§§ C. E. DeTar, J. Grunhaus,‖‖ E. S. Hafen,
R. I. Hulsizer, U. Karshon,¶¶ V. Kistiakowsky, A. Levy,‖‖ A. Napier, I. A. Pless,
J. P. Silverman, T. Stoughton, P. C. Trepagnier, J. Wolfson,*** and R. K. Yamamoto
Massachusetts Institute of Technology, Cambridge, Massachusetts 02139

H. O. Cohn
Oak Ridge National Laboratory, Oak Ridge, Tennessee 37830

P. F. Jacques, T. C. Ou, R. J. Plano, and T. L. Watts
Rutgers University, New Brunswich, New Jersey 08903

E. B. Brucker, E. Koller, P. Stamer, and S. Taylor
Stevens Institute of Technology, Hoboken, New Jersey 07030

W. M. Bugg, G. Condo, T. Handler, and E. Hart
University of Tennessee, Knoxville, Tennessee 37916

H. Kraybill, D. Ljung, T. Ludlam, and H. D. Taft
Yale University, New Haven, Connecticut 06520
(Received 16 June 1978)

The experimentally determined average charged-particle multiplicities, $\langle n_X \rangle$, of the systems, X, produced in the following reactions for 147 GeV/c incident pion momentum are presented as functions of the square of the invariant mass of X, M_X^2, and of $|t|$: $\pi^- p \to \pi_{\text{fast}}^- X$, $\pi^- p \to pX$, $\pi^- p \to \Delta^{++} X$, $\pi^- p \to (\pi^- \pi^+)_{\rho 0} X$, and $\pi^- p \to \Lambda^0 X$. Details of the analysis are discussed. These data can be fit by the expression $\langle n_X \rangle = A + B \ln M_X^2 + C|t|$ and the coefficients obtained for B are equal within their uncertainties. C is significantly different from zero only for $\pi^- p \to \pi_{\text{fast}}^- X$. These results and $\langle n_X \rangle$ data from other inclusive and total-inelastic-reaction studies are discussed in terms of a simple model which assumes contributions to $\langle n_X \rangle$ from the target-fragmentation, the central, and the beam-fragmentation regions in the case of total-inelastic reactions. For inclusive reactions, either the beam or target fragmentation is replaced by an exchange-particle-fragmentation contribution. The s, t, and M_X^2 dependence of the parameters of the model are deduced from triple-Regge considerations. The data are found to be consistent with the model and values are presented for the parameters.

I. INTRODUCTION

In this paper we present a study of the experimentally determined average charged-particle multiplicities, $\langle n_X \rangle$, of the systems, X, produced in the following reactions for 147 GeV/c incident pion momentum:

$$\pi^- + p \to \pi_{\text{fast}}^- + X^+ , \tag{1}$$

$$\pi^- + p \to p + X^- , \tag{2}$$

$$\pi^- + p \to \Delta^{++} + X^{--}, \qquad (3)$$

$$\pi^- + p \to (\pi^+ \pi^-)_{\rho^0} + X^0, \qquad (4)$$

$$\pi^- + p \to \Lambda^0 + X^0, \qquad (5)$$

These results were obtained with the Fermilab hybrid system[1,2] and a preliminary paper focusing on $\pi^- p \to \pi^-_{\text{fast}} X$ has already been published.[3]

The dependence of $\langle n_X \rangle$ from inclusive hadron-hadron reactions of the type

$$a + b \to c + X \qquad (6)$$

on various variables has previously been studied both theoretically and experimentally,[4-9] and compared with the average total charged-particle multiplicity in inelastic hadron-hadron reactions

$$a + b \to X. \qquad (7)$$

If $\langle n_X \rangle$ is given as a function of the square of the invariant mass, M_X^2, of the system X (which becomes in $a + b \to X$ just the square of the center-of-mass energy, s), then curves plotted for both $a + b \to c + X$ and $a + b \to X$ are very similar,[6-9] and approximately independent of the nature of particles a, b, and c and of the energy of the incident particle in $a + b \to c + X$. However, in our previous paper[3] we pointed out that there are small but significant systematic differences as a function of particle type and interpreted these differences in terms of a simple theoretical model.

In this study we present our final results for reactions (1) and (2), and give a complete description of the analysis of these data. We also present results for reactions (3)-(5) and discuss the average charged multiplicities for these five inclusive reactions and all other pertinent data from the literature in the context of the simple model. We begin with a brief review of previous theory and experiment in the second section of this paper. In the third section we describe our experiment and data analysis, and our results are presented in the fourth section. These are discussed in the context of the model in the fifth section, and summarized in the concluding section.

II. THEORETICAL AND EXPERIMENTAL BACKGROUND

The various theoretical models for multiparticle production which lead to predictions for the dependence of $\langle n_X \rangle$ on s in $a + b \to X$ have been discussed by Frazer *et al.*[10] and Feinberg.[11] They include the multiperipheral model and Regge-Mueller analysis which predict a linear dependence of $\langle n_X \rangle \propto s^a$ where $a > 0$. They also include the old Fermi statistical model and the Belenjki-Landau hydrodynamic model[11] which both predict $\langle n_X \rangle \propto s^{1/4}$. Subsequently, Garetto *et al.*[12] have proposed using the Polya-Eggenberger formula for

multiplicity distributions which also predicts $\langle n_X \rangle \propto s^{1/4}$, and Tow[13] has pointed out that inclusion of a secondary trajectory in a Regge-Mueller analysis predicts a term in $s^{-1/2}$ as well as one in $\ln s$. Figure 1 shows the data for the reaction

$$p + p \to X \qquad (8)$$

as a function of $\ln s$. It is qualitatively obvious that these data cannot be fit over the whole range of s by a simple linear dependence on $\ln s$. It has been shown that subsets of the data given in Fig. 1 can be fit by $A + B\ln s$,[13-16] $A + B (\ln s)^2$,[14] $A + B\ln s + C (\ln s)^2$,[14,16] $A + B\ln s + C s^{-1/2}$,[13,14] and $A s^{1/4}$.[14] Over the whole range of s only $A + B(\ln s)^2$, $A + B\ln s + C (\ln s)^2$, and $A + B\ln s + C s^{-1/2}$ give fits with reasonable χ^2 values.[14,17] The curve shown in Fig. 1 is the fit of $A + B\ln s + C (\ln s)^2$ to the data by Albini *et al.*[14]

Data also exist for

$$\pi^+ + p \to X^{++}, \qquad (9)$$

$$\pi^- + p \to X^0, \qquad (10)$$

$$K^+ + p \to X^{++}, \qquad (11)$$

$$K^- + p \to X^0, \qquad (12)$$

$$\bar{p} + p \to X^0, \qquad (13)$$

but for much more limited ranges of s. These may in general be fit by

$$\langle n_X \rangle = A + B\ln s \qquad (14)$$

as well as any of the other expressions which fit the data for $pp \to X$.[12,14,16,18] Furthermore, the values obtained for B in expression (14) are all between 0.9 and 1.4. Wroblewski[19] pointed out that if $\langle n_X \rangle$ were given as a function of "available energy," E_a, where
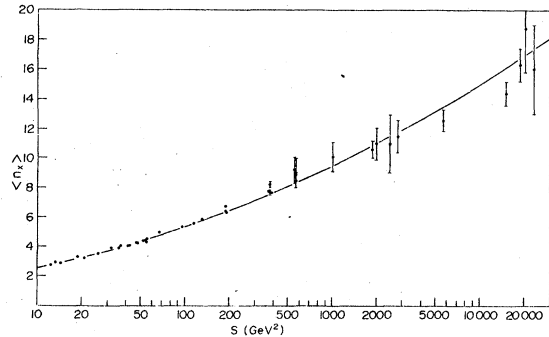
$$E_a = \sqrt{s} - M_a - M_b, \qquad (15)$$

FIG. 1. The average charged-particle multiplicity $\langle n_X \rangle$ as a function of s, for the reaction $pp \to X$. The data are from various sources, as quoted by Albini *et al.* in Ref. 14, and the curve shown is the fit to these data of $\langle n_X \rangle = A + B\ln s + C(\ln s)^2$, obtained in Ref. 14.

the data for $pp \to X$ and $\pi^- p \to X$ were very similar. Ammosov et al.[18] extended this approach and obtained a reasonably good simultaneous fit to data for $pp \to X$, $\pi^- p \to X$, and $K^- p \to X$ using the expression

$$\langle n_X \rangle = A + B \ln E_a + C(\ln E_a)^2 . \quad (16)$$

Turning to inclusive reactions, $a + b \to c + X$, an analogous situation is observed. A linear dependence of $\langle n_X \rangle$ on $\ln M_X^2$ has been predicted by several theoretical models such as the triple-Pomeron description[4] of the high-mass diffractive region $(10 < M_X^2 < s/10 \text{ GeV}^2/c^4)$ and the Amati-Bertocchi-Fubini-Stanghellini-Tonin multiperipheral model[5] for $M_X^2 > 20 \text{ GeV}^2/c^4$. Moreover, the slope of the linear increase of $\langle n_X \rangle$ has been predicted to be independent of s, t (the four-momentum transfer from $a \to c$), and the type of the incident particle, and to be identical to the slope of the linear increase with $\ln s$ of the average total charged multiplicity for $a + b \to X$. These predictions have previously been verified for the reaction

$$p + p \to p + X \quad (17)$$

at four energies,[6,7] and in $\pi^- p \to pX$ at 205 GeV/c.[8,9] In our previous paper, we reported the same result for $\pi^- p \to \pi_{\text{fast}}^- X$ and $\pi^- p \to pX$ at 147 GeV/c.[3]

Whitmore and Derrick[20] have extended the parametrization in terms of the available energy, E_a, to $a + b \to c + X$ where

$$E_a = M_X - M_b . \quad (18)$$

They point out that this is equivalent in a standard exchange picture to the reaction $E + b \to X$, where E is a virtual exchanged object (Pomeron, Reggeon, pion, or any combination of them). They obtain a roughly universal dependence of $\langle n_X \rangle$ on $\ln E_a^2$ for $\pi^- p \to pX$, $pp \to X$, $\pi^- p \to X$, and $pp \to pX$. In our previous paper[3] we have pointed out that there are significant differences between the data for $\pi^- p \to \pi_{\text{fast}}^- X$ and $\pi^- p \to pX$, and for $pp \to X$ and $\pi^- p \to X$ even when presented in terms of available energy. Pajares and Pascual[21] argue that the difference between $\pi^- p \to X$ and $pp \to X$ is due to differences in absorption between pions and protons. These differences are discussed further in the fifth section of this paper.

The various models for $a + b \to c + X$ also suggest a dependence of $\langle n_X \rangle$ on t, but do not predict a unique function form.[4,5] Studies of $\pi^- p \to pX$ and $pp \to pX$ at 205 GeV/c (Refs. 6, 9) and at the CERN ISR[22] do not indicate a significant t dependence in those reactions. Our previous paper[3] presented evidence for a significant t dependence in $\pi^- p \to \pi_{\text{fast}}^- X$ but not in $\pi^- p \to pX$. This will be discussed

further in the fourth section of this paper.

Finally, it should be point out that the linearity of the dependence of $\langle n_X \rangle$ on $\ln M_X^2$ (where $M_X^2 = s$ for total charged-particle multiplicities) has been observed not only for hadron-hadron interactions, but also for weak and electromagnetic processes.[23] The dependence on $\ln M_X^2$ of the average charged-particle multiplicities have similar slopes and their values at a given M_X^2 are also quite close for all three types of interactions. A universal rate of increase of the multiplicity with $\ln s$ is explained in some quark models[24] and a one-dimensional field theoretical model.[25] The multiperipheral and Mueller-Regge models[14] also give a universal rate of increase for total and associated multiplicities in hadronic collisions but they are not directly applicable to $e^+ e^-$ annihilation. In the model of Brodsky and Gunion[24] the $\ln s$ dependence arises from an underlying gluon-bremstrahlung process, and the universal rate from the assumption that the bremstrahlung sources are color-triplet fragments of the beam and target. In the other models, the universality of the $\ln s$ growth arises from the assumption that the emission of the secondaries is essentially independent of the nature of the beam and target particles, leading to a uniform distribution of the secondaries in longitudinal phase space.

In contrast to a widespread theoretical consensus about the universal asymptotic rate of growth of the average multiplicity, there are no solid theoretical predictions about the dependence of the constant term A in Eq. (14) upon the beam and target type. Such a prediction depends too intimately upon the dynamical details of particle production for current elucidation.

III. DATA ANALYSIS

A. General discussion

This experiment consisted of an exposure of 105 000 pictures of 147 GeV/c π^- mesons in the Fermilab 30-inch bubble-chamber hybrid spectrometer. Details of the experimental arrangement and the data reduction in this experiment have already been published.[1,2] Table I gives the number of events corresponding to the various samples that will be discussed in this paper. The topological cross sections have been presented in a previous paper.[2] To obtain the average charged multiplicities for reactions (1)–(5), it is necessary to correct the number of usable events in the various topologies for scanning and processing losses by appropriate topology dependent weights.[26] These weights depend to some extent on the reaction type in question and are discussed in the following paragraphs. An event is defined

TABLE I. Number of events and total cross sections for the various samples of this experiment, $\pi^- p$ at 147 GeV/c.

Sample	Number of events	Cross section (mb)
$\pi^- p \to \pi_{\text{fast}}^- X$	1867	5.15 ± 0.12
$\to pX$	2601	8.01 ± 0.42
$\to \Delta^{++} X$	471	1.13 ± 0.16
$\to (\pi^+ \pi^-) \rho^0 X$	1064	3.74 ± 0.12
$\to \Lambda^0 X$	238	1.65 ± 0.21
$\to X$ (inelastic)	7218	21.00 ± 0.32

to be usable if it is in one of two categories: (1) all tracks are properly measured and fitted, and their net charge is zero (charge balance); (2) one or more tracks are not measured or fitted, but the event is consistent with charge balance (neither the number of measured and fitted positive tracks nor the number of measured and fitted negative tracks is greater than half the scanner prong count). The third class, charge-unbalanced events, were not used and constituted 4.6% of the total inealstic sample. Within the uncertainties they were uniformly distributed among the topologies. There was also a large sample of events (4253) which were rejected by the geometry program (GEOMAT).[2] Since these losses occurred more heavily in the higher multiplicities (13.6% of all two prongs was rejected and 49.6% of all twelve prongs), the events lost to this category are a possible source of bias which was studied in a manner relevant to the particular reaction type.

Another source of bias inherent in the use of the topology-dependent weights arises from the inability to detect very-low-momentum protons in two-prong inealstic events. The $d\sigma/dt$ vs t distribution for two-prong inelastic events with identified protons was fit by e^{bt} for $|t| \geq 0.04$ GeV^2 and the exponential was extrapolated to $t = 0$. This extrapolation showed that $60 \pm 5\%$ of the events with $|t| < 0.04$ GeV^2 were missed. Therefore, separate topology dependent weights were used for two-prong events with identified protons with $|t| < 0.04$ (GeV^2), for those with identified protons with $|t| \geq 0.04$ GeV^2 and for those without identified protons. The latter category includes both events with protons for which ionization identification was not possible ($p_{\text{lab}} > 1.4$ GeV/c) and events with a neutron, and constitutes 47% of the two-prong inelastic sample. These two-prong topology weights were used in the study of reactions (1) through (5) but only produced significant differences in the t distributions for $\pi^- p \to pX$.

B. $\pi^- p \to \pi_{\text{fast}}^- X$

A usable event was included in the sample for $\pi^- p \to \pi_{\text{fast}}^- X$ if it contained a negative particle with $X \geq 0.50$.[27] This limit corresponds to $M_X^2 \lesssim 140$ GeV^2/c^4. The momentum of the fast negative particle is determined by its deflection in the bubble-chamber magnet as measured in the downstream proportional wire system.[2] In order to determine whether the sample was biased by the loss of events which failed to be reconstructed in the bubble chamber (geometry rejects), a special measurement of beam track and vertex was made on a sample of such rejects. The downstream proportional-wire-chamber (PWC) data were then used to reconstruct forward going tracks associated with these vertices, and the fraction of these events which had a fast negative particle with $x \geq 0.5$ was determined. Within the uncertainties, this fraction, about 50%, was the same for the rejected events as for the usable events at all multiplicities. Therefore, these lost events do not introduce a bias.

The uncertainty in the momentum measurements in the downstream PWC system is $\Delta p/p = 6 \times 10^{-4} p$ with p in units of GeV/c, and 18% of the fast pions had measured momenta greater than the beam momentum. For such events a calculation of the invariant mass squared, M_X^2, gives $M_X^2 < 0$. The uncertainties on M_X^2 for these events are very large and increase rapidly as a function of the measured momentum of the pion. The average charged multiplicity of these events is lower than that of the whole sample. If, however, the $M_X^2 < 0$ events are compared with those for which $0 < M_X^2 < 20$ GeV^2/c^4, the average charged multiplicities are in agreement within uncertainties for the whole range of $|t|$. This suggests that most of the observed $M_X^2 < 0$ events come from real $0 < M_X^2 < 20$ GeV^2/c^4 events, a hypothesis which is supported by the observation that the distribution of uncertainties in M_X^2, for events with $M_X^2 > 0$, is peaked at 12 GeV^2/c^4. The method which was used to treat the $M_X^2 < 0$ events was to reduce the magnitude of the momentum of the charged secondaries by an amount equal to $w_i \cdot \delta |\vec{p}|$, where $w_i = \Delta p_i / \sum_{\text{out}} \Delta p_j$ is the weighting factor for the ith particle and Δp_i is the momentum uncertainty for the particle, and where $\delta |\vec{p}| = |\sum_{\text{out}} \vec{p}_i| - |\vec{p}_{\text{beam}}|$ is the charged particle momentum imbalance, p_i are the momenta of the outgoing particles, and p_{beam} is that of the beam pion. This correction does not take possible neutral production into consideration, but is designed to distribute the momentum imbalance according to the uncertainty of the momentum determinations. The validity of this procedure has been
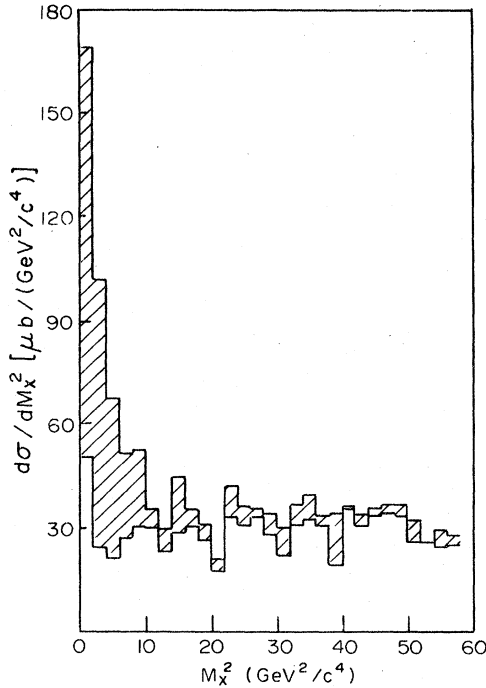
FIG. 2. The differential cross section, $d\sigma/dM_X^2$, vs M_X^2 for $\pi^- p \rightarrow \pi^-_{\text{fast}} X$ at 147 GeV/c. The unshaded area gives the uncorrected distribution in M_X^2, while the shaded area shows the contribution from the $M_X^2 < 0$ events, described in the text. This contribution is negligible above $M_X^2 = 60$ MeV^2/c^4.

verified by Monte Carlo tests. It results in a shift of 73% of the $M_X^2 < 0$ events to the $0 < M_X^2 < 20$ GeV^2/c^4 region, and 18% to $M_X^2 > 20$ GeV^2/c^4. Figure 2 gives the corrected distribution of events as a function of M_X^2 for $\pi^- p \rightarrow \pi^-_{\text{fast}} X$ and shows separately the contribution from the $M_X^2 < 0$ events for $M_X^2 \leqslant 60$ GeV^2/c^4, the region populated by these events. These events have a negligible effect on the other distributions given in this paper.

C. $\pi^- p \rightarrow pX$

A usable event was included in the sample for $\pi^- p \rightarrow pX$ if it contained a positive particle identified on the basis of range or ionization as a proton. This is possible up to proton momentum of 1.4 GeV/c, where the proton ionization is 1.45 times the ionization of a beam track. No particles with $p > 1.4$ GeV/c were taken as protons. This proton-momentum limit corresponds to $|t| < 1.4$ GeV^2, $x \lesssim -0.3$, and $M_X^2 \lesssim 200$ GeV^2/c^4. Since the proton identification in the momentum region 1. to 1.4 GeV/c has ~25% uncertainty and since no proton events are included for $p > 1.4$ GeV/c, the samples for $M_X^2 \gtrsim 140$ GeV^2/c^4 may be some-

what biased by inclusion of some events with pions misidentified as protons and exclusion of real proton events.

A comparison was made between distributions for all $\pi^- p \rightarrow pX$ events as defined above and distributions for these events which also satisfied the condition $|x| \geqslant 0.5$—the condition used for $\pi^- p \rightarrow \pi^-_{\text{fast}} X$. The only effect caused by the x cut was a statistically insignificant change in distributions for $120 < M_X^2 \leqslant 140$ GeV^2/c^4 and, of course, the absence of events in higher-M_X^2 bins. Thus, the results shown in this paper are given for the data without a cut on x.

The geometry rejects were studied on scanning tables and found to contain more protons (identified visually by ionization) than the sample of usable events. This was not found to be topology dependent within the uncertainties and, therefore, a correction factor of 1.05 ± 0.05 was included in the weights for all topologies to take account of the loss of events containing protons.

Since the weights for topologies with high prong numbers are large and the number of usable high
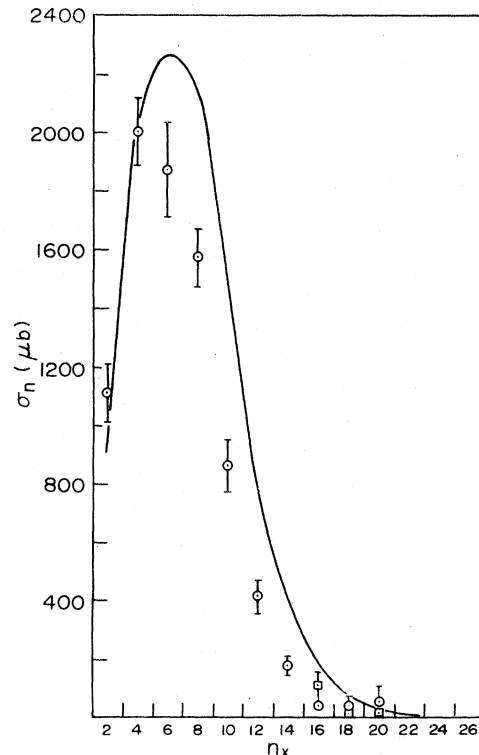

FIG. 3. Topological cross sections, σ_n, vs n_X for $\pi^- p \rightarrow pX$ at 147 GeV/c, obtained by two different methods for correcting high multiplicity events for topology-dependent measuring losses, as described in the text; smoothed, $\boxdot$, and unsmoothed weighted, $\odot$. The solid curve is $\frac{1}{2}\sigma_n$ vs n_X for the overall inclusive reaction $\pi^- + p \rightarrow X$.

multiplicity events for $\pi^- p \to pX$ is small, these events cause noticeable fluctuations and do not adequately represent the true situation. Therefore, distributions were obtained using two different weighting schemes. The first method ignores the 20–26 prong events entirely and uses the appropriate topology dependent weights for the 16 and 18 prong events. The second method places all topologies with 16 or more prongs in a single category. All differences observed between the results for the two methods were within one standard deviation, but the second method smoothed out fluctuations observed in the results obtained with the first method. Figure 3 gives the topological cross section for $\pi^- p \to pX$ with and without the smoothed weighting.

D. $\pi^- p \to \Delta^{++} X$

The analysis of the data to obtain the sample for $\pi^- p \to \Delta^{++} X$ has been discussed in a previous publication.[28] Summarizing the criteria, events are included in this sample if they satisfy those for $\pi^- p \to pX$ and if there is a $\pi^+ p$ system with an invariant mass, $M_{p\pi^+}$, in the region $1.14 < M_{p\,\pi^+} < 1.30$ GeV/c^2. If there is more than one $\pi^+ p$ combination in a given event which satisfies the latter criterion, the combination for which the π^+ has the lowest rapidity is taken. Finally, the momentum transfer from proton to Δ^{++}, $t_{p\Delta^{++}}$, is calculated and events with $|t_{p\Delta^{++}}| > 1.0$ GeV^2 are discarded.

E. $\pi^- p \to (\pi^+\pi^-)_{\rho^0} X$

The production of ρ^0 mesons in this experiment has been discussed in a previous publication,[29] but the analysis used in this paper was necessarily different since statistics precluded fitting the distributions of the $\pi^+\pi^-$ invariant mass, $M_{\pi^+\pi^-}$ from $\pi^- p \to \pi^+\pi^- X$ for the various M_X^2 and $|t|$ regions with Breit-Wigner and polynomial background terms. Figure 4 gives the $\pi^+\pi^-$ invariant mass distributions for $\pi^+\pi^-$ pairs satisfying the requirement $x_{\pi^+\pi^-} > 0.5$ for various topologies. The $x_{\pi^+\pi^-}$ requirement assures that we are in the kinematic region corresponding to the beam fragmentation region and also increases the ratio of resonance to background. Clear resonance signals are observed in Fig. 4, even at higher multiplicity topologies, but there is a non-negligible amount of background beneath these peaks. Consequently, we have taken all events satisfying both the requirement $x_{\pi^+\pi^-} > 0.5$ and $0.5 \leq M_{\pi^+\pi^-} \leq 1.0$ GeV/c^2 for the $\pi^- p \to (\pi^+\pi^-)_{\rho^0} X$ sample, and also present comparisons with data from the neighboring regions, $0.26 \leq M_{\pi^+\pi^-} < 0.5$ GeV/c^2 and $1.0 < M_{\pi^+\pi^-} \leq 1.4$ GeV/c^2, to elucidate the effect of the background.
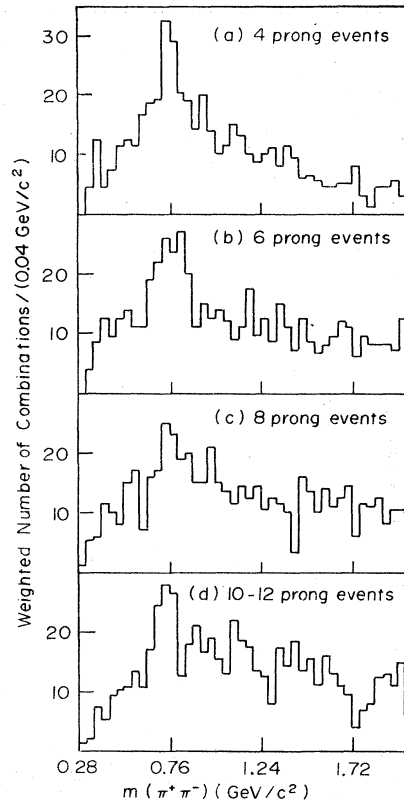

FIG. 4. Distributions in $\pi^+\pi^-$ invariant mass, $M_{\pi^+\pi^-}$, for the reaction $\pi^- p \to \pi^+\pi^- X$ at 147 GeV/c, plotted separately for different total charged-particle multiplicities. Only events having $X_{(\pi^+\pi^-)} \geq 0.5$ are included.

F. $\pi^- p \to \Lambda^0 X$

The analysis of the data necessary to obtain the $\pi^- p \to \Lambda^0 X$ events will be presented in a future paper.[30] The events included in this sample were events that gave three constraint fits (87%) or one constraint fits (13%) to Λ^0 hypotheses. Twenty percent of these events also could be fit by either the K^0 or $\bar{\Lambda}^0$ hypotheses and were assigned to the Λ^0 sample on the basis of relative chi squares, χ^2. The weights used in determining the cross sections and average multiplicities include factors for decay probability, branching ratio, scan efficiency, and measuring efficiency.

IV. EXPERIMENTAL RESULTS

A. $\pi^- p \to \pi_{fast}^- X$ and $\pi^- p \to pX$

The cross sections as functions of charged-particle multiplicity for $\pi^- p \to \pi_{fast}^- X$ and $\pi^- p \to pX$ are given in Figs. 5 and 3. The solid curve shows the topological cross sections for $\pi^- p \to X$.[2] Notice that both inclusive distributions are significantly narrower than the total topological distri-

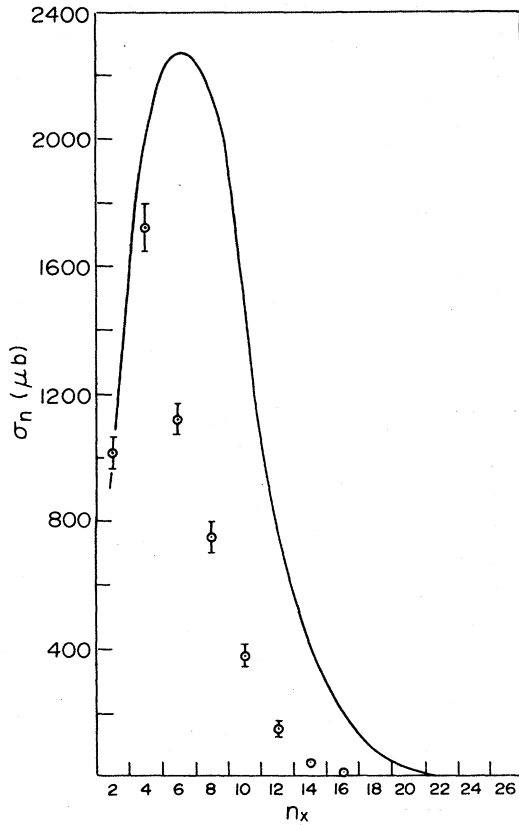FIG. 5. Topological cross sections, σ_n, vs n_X for $\pi^- p \to \pi^-_{\text{fast}} X$ at 147 GeV/c. The solid curve represents $\frac{1}{2}\sigma_n$ vs n_X for the overall inclusive reaction $\pi^- p \to X$ at 147 GeV/c.

bution. This fact is probably due to the peripheral nature of the inclusive reactions which yields lower multiplicities.

Figure 6 gives the differential cross section for $\pi^- p \to \pi^-_{\text{fast}} X$ as a function of $|t|$ for various M_X^2 intervals. The result for $M_X^2 < 20$ GeV$^2/c^4$ contains most of the events for which $M_X^2 < 0$, as discussed in the previous section. The result for all M_X^2 [Fig. 6(a)] is clearly not a simple exponential. However, the differential cross sections for each of the various M_X^2 intervals have been fit for the low $|t|$ region by an exponential, $e^{-b|t|}$. The parameter, b, is given in Fig. 7 as a function of M_X^2, together with a straight line calculated from the results of a linear fit to the data for $M_X^2 > 20$ GeV^2. The coefficient of the M_X^2 term obtained in this fit was -0.029 ± 0.010, within 3 standard deviations of zero.

Figure 8 gives the differential cross section for $\pi^- p \to pX$ as a function of t' for various M_X^2 intervals, where $t' = |t - t_{\min}|$ and $t_{\min}$ is the minimum value of t. The variable t' is used rather than t in order to eliminate kinematic effects due
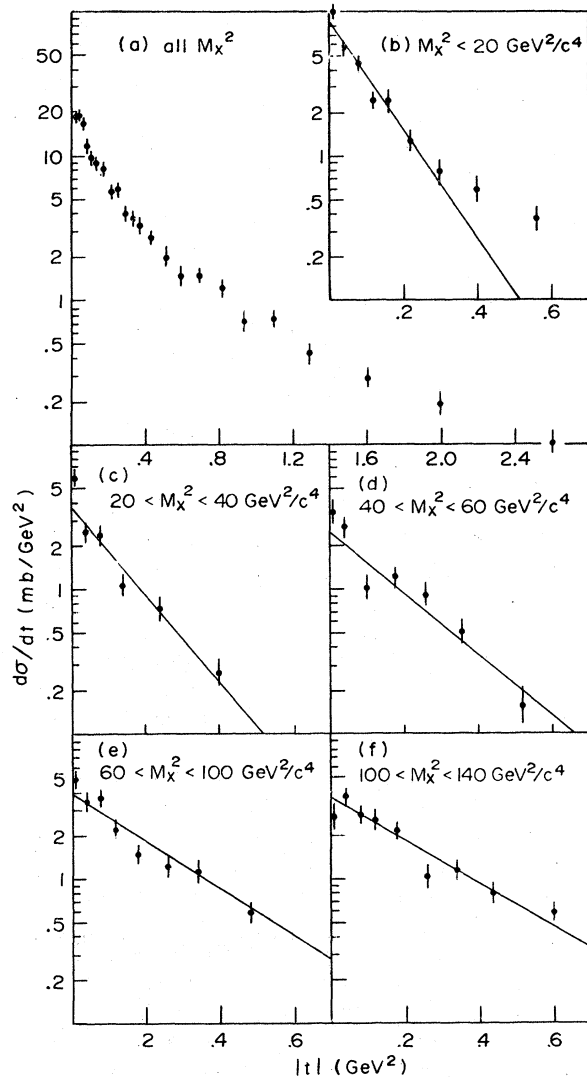

FIG. 6. The differential cross section, $d\sigma/dt$, as a function of t for $\pi^- p \to \pi^-_{\text{fast}} X$ at 147 GeV/c. (a) shows $d\sigma/dt$ for all M_X^2, while (b)–(f) show $d\sigma/dt$ for various intervals of M_X^2. The lines are plots of exponential fits of the form, $d\sigma/dt = A^{-b|t|}$, to the data.

to the Chew-Low boundary. The data in the various M_X^2 intervals were fit by exponentials, $e^{-b'|t'|}$, and the lines corresponding to these fits are also shown in Fig. 8. Figure 9 gives the value of b' as a function of M_X^2 for the fits shown in Fig. 8 and for the values of b obtained from fits of the same data to $d\sigma/dt = ae^{-b|t|}$. The values of b and b' are the same for any given M_X^2 within the uncertainties. Also shown in Fig. 9 is the line calculated from parameters obtained by fitting the results for b' with a linear dependence on M_X^2 for $M_X^2 > 20$ GeV$^2/c^4$. As is the case for $\pi^- p \to \pi^-_{\text{fast}} X$, the dependence of b on M_X^2 is only a 3-standard-
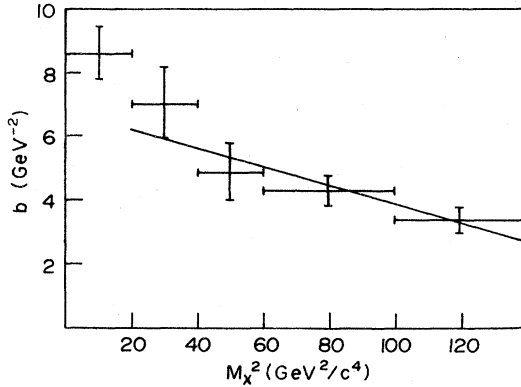
FIG. 7. The parameter b from the exponential fits, $d\sigma/dt = ae^{-b|t|}$, of Fig. 6(b)–6(f) as a function of M_X^2. The solid line is calculated from a fit to these points, for $M_X^2 > 20$ GeV^2/c^4, of the linear relation $b = (6.8 \pm 1.0) - (0.029 \pm 0.010) M_X^2$.

deviation effect, -0.026 ± 0.008, but that of b', -0.027 ± 0.003, is significant. The shrinkage of $b(b')$ with the mass of the relevant system is a well-known effect from lower energies[31] and it is interesting to note that this persists up to 147 GeV/c.

The differential cross section as a function of M_X^2, $d\sigma/dM_X^2$, for $\pi^- p \rightarrow \pi_{\text{fast}}^- X$ is given in Fig. 2 for all t and in Fig. 10 for various t intervals. That for $\pi^- p \rightarrow pX$ is given in Fig. 11. The low-mass diffractive peak seen in the distributions for $|t| < 0.3$ GeV^2 disappears for higher values of $|t|$. As has been pointed out previously, the main contributions to the diffractive peak come from the two- and four-prong topologies.[4,8] There is a depletion of $d\sigma/dM_X^2$ for large values of M_X^2 in $\pi^- p \rightarrow pX$ due to the upper limit of 1.4 GeV/c on the proton momentum.

Figure 12 shows the average charged multiplicity, $\langle n_X \rangle$, for $\pi^- p \rightarrow \pi_{\text{fast}}^- X$ as a function of M_X^2 for various intervals of t. The solid lines give the result of the best fit of the expression

$$\langle n_X \rangle = A + B \ln M_X^2 \qquad (19)$$

to the data for $M_X^2 > 20$ GeV^2 in each t interval. Figure 13(a) gives the values obtained for B as a function of $|t|$. A fit of the expression

$$B = D + E|t| \qquad (20)$$

to these results gave $E = 0.48 \pm 0.21$, and the line corresponding to this fit is shown on Fig. 13(a). Although this result indicates a weak dependence of B on $|t|$, it is also consistent within 2.3 standard deviations with the absence of a t dependence.

Figure 14 gives $\langle n_X \rangle$ for $\pi^- p \rightarrow \pi_{\text{fast}}^- X$ as a function of $|t|$ for various M_X^2 intervals. The distri-
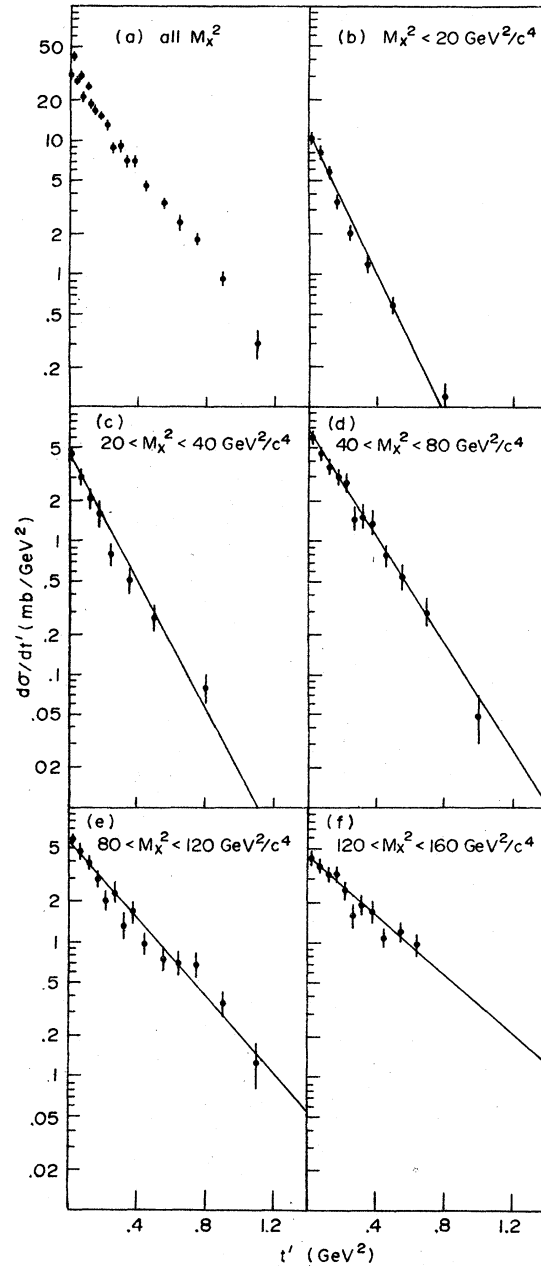

FIG. 8. The differential cross section, $d\sigma/dt'$, as a function of t' for $\pi^- p \rightarrow pX$ at 147 GeV/c. (a) shows the data for all M_X^2, while (b)–(f) present the data for various intervals in M_X^2. The lines are plots of exponential fits of the form, $d\sigma/dt' = ae^{-b't'}$, to the data in each interval.

bution in the proton diffraction region ($M_X^2 < 20$ GeV^2/c^4) is seen to have a t dependence similar to the higher M_X^2 intervals; however, $\langle n_X \rangle$ is lower by ~ 2 units for the proton diffraction region than for the higher M_X^2 region. The increase of $\langle n_X \rangle$ with $|t|$ for the region $M_X^2 < 20$ GeV^2/c^4,
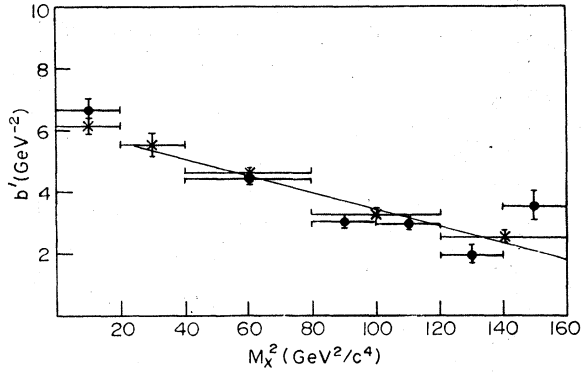
FIG. 9. The values of the parameter b' from the exponential fits, $d\sigma/dt' = ae^{-b't'}$, of Fig. 8(b)–8(f) are given as a function of M_X^2 by the crosses. The solid line is calculated from a fit to these points for $M_X^2 > 20$ GeV^2/c^4 of the linear relation $b' = (6.16 \pm 0.26) - (0.0267 \pm 0.0028) M_X^2$. The solid circles give equivalent results from fits of $d\sigma/dt = ae^{-b|t|}$ to the $\pi^- p \to pX$ data.

which is dominated by diffractively produced N^{*}'s, is consistent with the established observations that $d\sigma/dt$ for low-mass N^{*}'s decreases faster with $|t|$ than that for high-mass N^{*}'s and that the more massive N^{*}'s decay into higher multiplicities.[32] The solid lines give the result of the

FIG. 11. The differential cross section, $d\sigma/dM_X^2$, as a function of M_X^2, for various intervals of $|t|$, for $\pi^- p \to pX$ at 147 GeV/c.
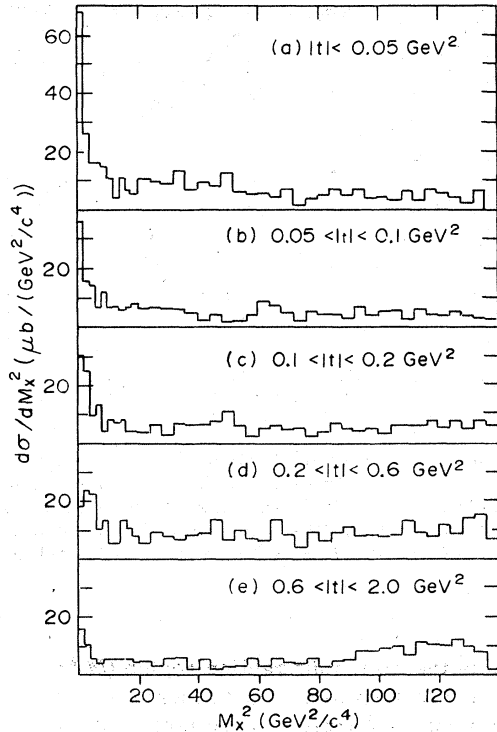

FIG. 10. The differential cross section, $d\sigma/dM_X^2$, as a function of M_X^2, for various intervals of $|t|$, for $\pi^- p \to \pi^-_{\text{fast}} X$ at 147 GeV/c.
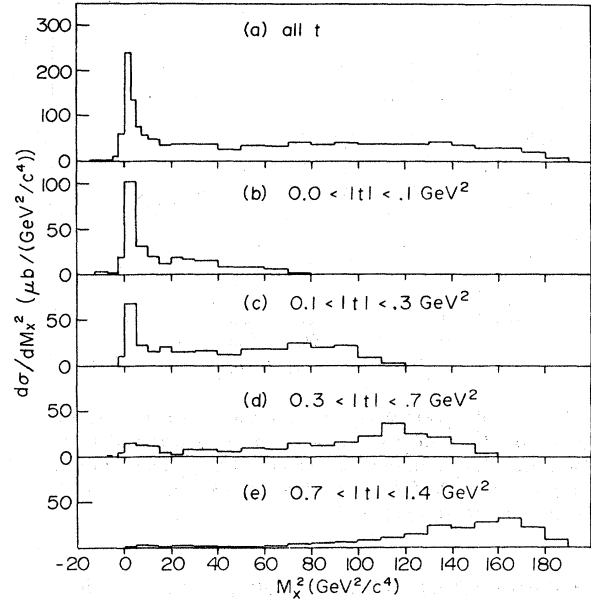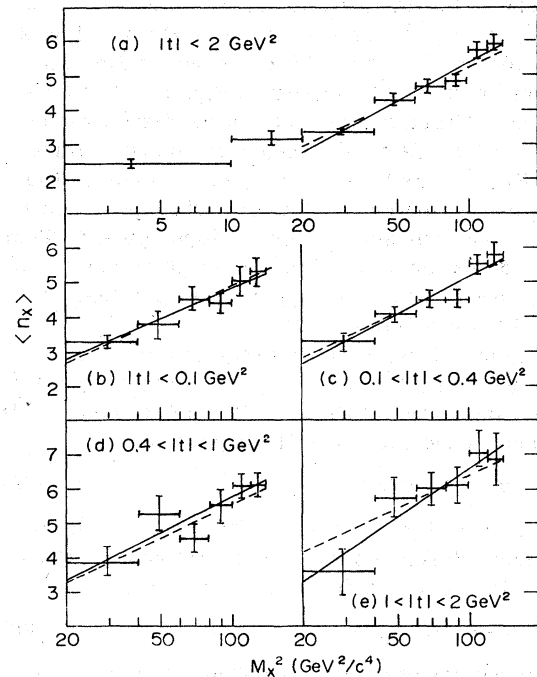

FIG. 12. The average charged-particle multiplicity $\langle n_X \rangle$ for $\pi^- p \to \pi^-_{\text{fast}} X$ at 147 GeV/c, plotted as a function of M_X^2 for various intervals in $|t|$. The solid lines are plots of the best fits to the data for $M_X^2 > 20$ GeV^2/c^4 in the respective $|t|$ intervals of expression (19). The dashed lines are plots of two-variable fits of expression (23), evaluated with $|t|$ equal to the mean value for the given interval.
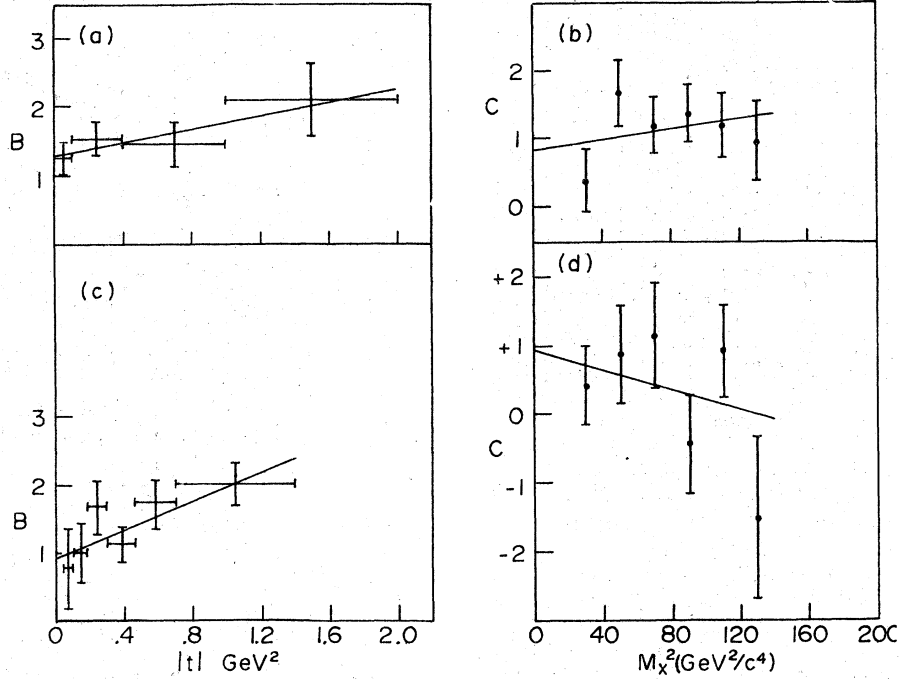
FIG. 13. (a) The values obtained for B from a fit of expression (19) to the data in Fig. 12, as a function of $|t|$. The line gives the results of a fit of expression (20). (b) The values obtained for C from a fit of expression (21) to the data in Fig. 14, as a function of M_X^2. The line gives the results of a fit of expression (22). (c) The values obtained for B from a fit of expression (19) to the data in Fig. 15, as a function of $|t|$. The line gives the results of a fit of expression (20). (d) The values obtained for C from a fit of expression (21) to the data in Fig. 16, as a function of M_X^2. The line gives the result of a fit of expression (22).

best fit of the expression

$$\langle n_X \rangle = A + C|t| \tag{21}$$

to the data in that particular M_X^2 interval. Figure 13(b) presents C as a function of M_X^2 and it is seen that there is a significant t dependence which is the same within the uncertainties for all M_X^2 intervals. A fit of the expression

$$C = D + FM_X^2 \tag{22}$$

to these results gave $F = 0.004 \pm 0.006$, and the line corresponding to this fit is shown in Fig. 13(b).

Since $\langle n_X \rangle$ for $\pi^- p \rightarrow \pi^-_{\text{fast}} X$ can be fit by a linear dependence on $\ln M_X^2$ and on $|t|$ and since the coefficient for the dependence on one variable can be considered independent of the other, a two-variable fit of the expression

$$\langle n_X \rangle = A + B \ln M_X^2 + C|t| \tag{23}$$

was carried out. The values obtained for the coefficients are given in Table II and the results calculated from them are shown by the dashed lines in Figs. 12 and 14. These results and others given in this section differ slightly from those in Ref. 3 due partially to subsequent additions to the data sample and improvements in the analysis, but also more substantially to changes in binning.

Figure 15 gives the dependence of $\langle n_X \rangle$ for $\pi^- p \rightarrow p X$ on M_X^2 for various $|t|$ intervals. As previously discussed, the data for $M_X^2 > 140 \, \text{GeV}^2/c^4$ may be subject to some uncertainties and therefore the results for $20 < M_X^2 < 140 \, \text{GeV}^2/c^4$ were fit by expression (19). The parameters obtained from this fit are given in Fig. 13(c) as function of $|t|$ and the solid lines in Fig. 15 are calculated from them. Again, as for $\pi^- p \rightarrow \pi^-_{\text{fast}} X$, the values obtained for B are the same within three standard deviations. A fit of $B = D + E|t|$ to these values gave $E = 1.03 \pm 0.35$ and the line in Fig. 13(c) shows the result of this fit.

Figure 16 gives the dependence of $\langle n_X \rangle$ for $\pi^- p \rightarrow p X$ on $|t|$ for various M_X^2 intervals. These data were fit by $\langle n_X \rangle = A + C|t|$ and the values of C obtained are given in Fig. 13(d). The solid lines in Fig. 16 are calculated from these results. The results obtained for C are consistent with the absence of a significant $|t|$ dependence of $\langle n_X \rangle$. When the values obtained for C are fit by $C = D + FM_X^2$, the result obtained is $F = -0.007 \pm 0.010$, indicating no M_X^2 dependence for C. The line in Fig. 13(d) is calculated from this fit. This analysis was also carried out using $|t'|$ as a variable and the same result was obtained.

Since the coefficients B and C for $\pi^- p \rightarrow p X$ can be considered independent of $|t|$ and M_X^2, respec-
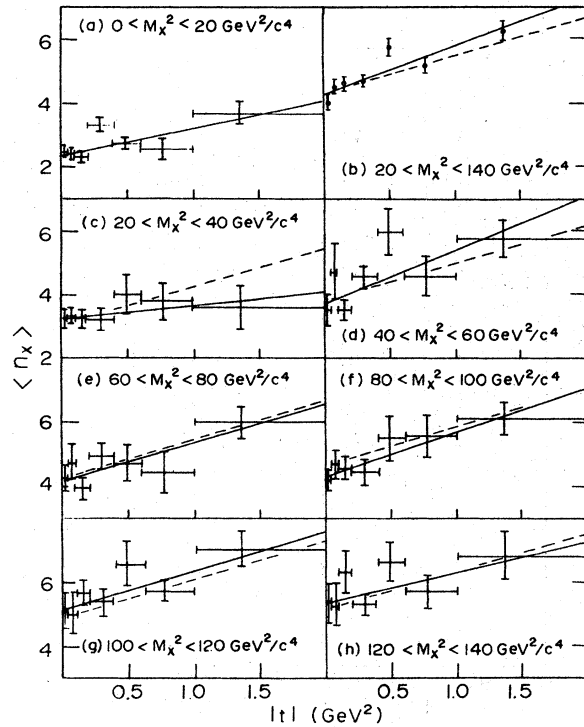
FIG. 14. The average charged-particle multiplicity $\langle n_x \rangle$ for $\pi^- p \to \pi^-_{fast} X$ at 147 GeV/c, as a function of $|t|$ for various intervals in M_X^2. The solid lines give the results of the best fits to the data in the respective M_X^2 regions of expression (21). The dashed lines are plots of two variable fits of expression (23), evaluated with M_X^2 equal to the mean value for the given interval.

FIG. 15. The average charged-particle multiplicity $\langle n_x \rangle$ for $\pi^- p \to pX$ at 147 GeV/c, as a function of M_X^2 for various intervals in $|t|$. The solid lines are plots of the best fits to the data for $M_X^2 > 20$ GeV^2/c^4 in the respective regions of $|t|$ of expression (19). The dashed lines are plots of two-variable fits of expression (23), evaluated at the average value of $|t|$ for the given interval.

tively, the data were fit by $\langle n_x \rangle = A + B \ln M_X^2 + C|t|$. The parameters obtained in the fit are given in Table III and the dashed lines in Figs. 15 and 16 show the results calculated from them. The value found for C is consistent with zero within 2.5 standard deviations and B for $\pi^- p \to pX$ is seen to be the same as B for $\pi^- p \to \pi^-_{fast} X$ within the uncertainties. These results are in agreement with the value obtained for B from a fit of expression (19) to data at 205 GeV/c and with the observation that
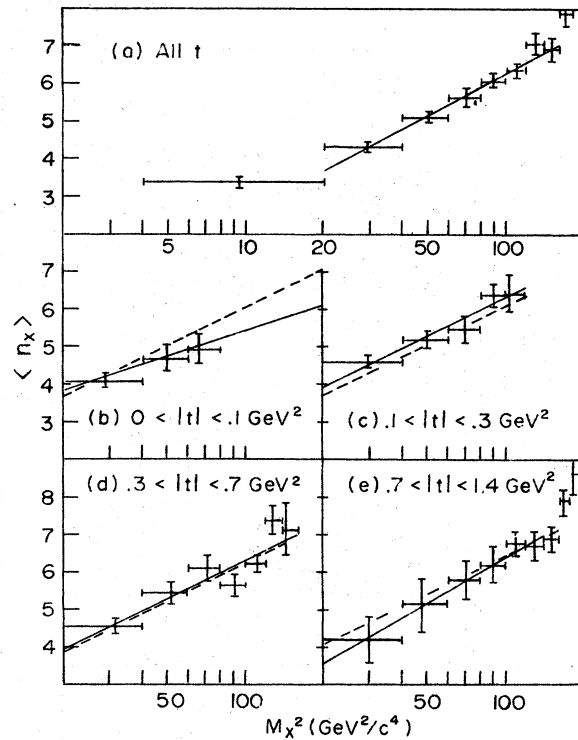
there is no significant t dependence at that energy.[9]

In order to check the uniqueness of a fit of $\langle n_x \rangle = A + B \ln M_X^2$ or $\langle n_x \rangle = A + B \ln M_X^2 + C|t|$ to these data, other forms suggested in the literature were also tried. Some of these results are given in Tables II and III and it is seen that all of the expressions used except that with a $\ln [1/(1 + |t|)]$ dependence also give acceptable fits to our data

TABLE II. Parameters obtained by fits of the indicated expressions to $\langle n_x \rangle$ data for $\pi^- p \to \pi^-_{fast} X$ at 147 GeV/c for $20 \le M_X^2 \le 140$ GeV^2/c^4 and $|t| < 2.0$ GeV^2.

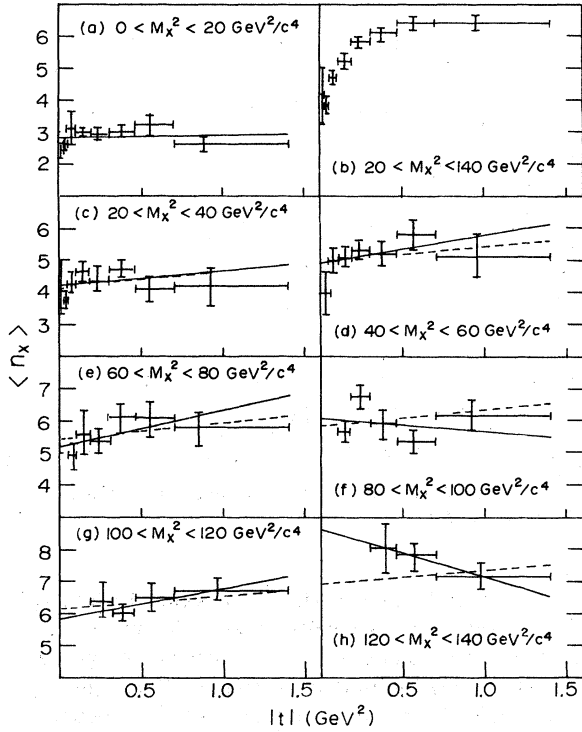| Expression	A	B	C	D	χ^2/ND
$A + B \ln M_X^2 + C|t|$	-2.11 ± 0.55	1.50 ± 0.14	1.15 ± 0.18		1.43
$A + B \ln M_X^2 + C(\ln M_X^2)^2$	8.82 ± 5.84	-3.83 ± 2.89	0.67 ± 0.35		1.19
$A + B M_X$	1.17 ± 0.33	0.42 ± 0.04			1.01
$A + B \ln(M_X^2/(1 + |t|))$	0.29 ± 0.51	1.08 ± 0.13			4.66
$A + B \ln M_X^2 + C|t|^{1/2}$	-2.36 ± 0.56	1.48 ± 0.14	1.52 ± 0.24		1.39
$A + B \ln M_X^2 + Ce^{-D|t|}$	-0.04 ± 1.84	1.48 ± 0.14	-2.15 ± 1.74	0.88 ± 0.80	1.44

FIG. 16. The average charged-particle multiplicity
$\langle n_X \rangle$ for $\pi^- p \to p X$ at 147 GeV/c, as a function of $|t|$
for various intervals in M_X^2. The solid lines are plots
of the best fits to the data in the respective M_X^2 regions
of expression (21). The dashed lines are plots of two-
variable fits of expression (23), evaluated at the aver-
age value of M_X^2 for the given interval.

for $\langle n_X \rangle$.

Figure 17 shows the results obtained for the
Mueller parameter f_2,[33] for $\pi^- p \to \pi_{\text{fast}}^- X$, both as a
function of M_X^2 and of $|t|$. The line is calculated
from the results of a fit to the data for $\pi^- p \to X$ of
a quadratic expression in ln s.[15] Unfortunately,
the uncertainties on our data are too large for a
significant fit, but it can be seen that f_2 increases
with M_X^2 in a manner not inconsistent with such a
dependence.

Figure 18 gives the results for f_2 for $\pi^- p \to p X$
as a function of M_X^2 and of t. The M_X^2 dependence
is qualitatively the same as that observed for
$pp \to p X$ at several energies.[34]

B. $\pi^- p \to \Delta^{++} X$

Figure 19 presents the differential cross sec-
tion for $\pi^- p \to \Delta^{++} X$ as a function of M_X^2 for
various $|t|$ intervals. The cross sections for
four-prong events with no neutral particles (i.e.,
events for which a four-constraint (4C) fit was
possible) are indicated by the shaded areas. As
has been shown in a previous publication,[28]
these events are mainly quasielastic N^{*+} produc-
tion (with the N^{*+} decaying to $\pi^- \Delta^{++}$). Thus, in
order to study $\pi^- p \to \Delta^{++} X$ without $\pi^- p \to N^{*+} X$,
these events were deleted from the data from
which the $\langle n_X \rangle$ presented in Figs. 20 and 21 were
calculated. However, the results without the de-
letion of these events were the same, well within
the uncertainties. Figure 20 gives $\langle n_X \rangle$ as a func-
tion of M_X^2 and Fig. 21 as a function of $|t|$. The
dashed lines are calculated from the results of a
fit of $\langle n_X \rangle = A + B \ln M_X^2 + C|t|$ to these data. The
coefficients which were obtained are given in
Table IV. Although the $|t|$ dependence is similar
to that for $\pi^- p \to p X$, it is only a 1-standard-devia-
tion effect.

C. $\pi^- p \to (\pi^+ \pi^-) \rho^0 X$

The values obtained for $\langle n_X \rangle$ for the ρ^0 sample
$(X_{\pi^+\pi^-} - \geq 0.5$ and $0.5 \leq M_{\pi^+\pi^-} \leq 1.0$ GeV/c^2) as a
function of M_X^2 are given in Fig. 22(a) and those
for the background region $(x_{\pi^+\pi^-} \geq 0.5$ and $0.26 \leq M_{\pi^+\pi^-} < 0.5$
GeV/c^2 plus $1.0 < M_{\pi^+\pi^-} \leq 1.4$ GeV/c^2) are given in
Fig. 22(b). In a very detailed analysis of $\pi^- p
\to \rho^0 X$ at 15 GeV/c, it has recently been shown
that ρ^0 production in the incident π^- fragmen-
tation region is mainly due to π exchange.[35]
Thus, it is interesting to compare the results
from this experiment which apparently involve
off-shell "$\pi^- $"$p \to X$ with $\langle n_X \rangle$ as a function of s for
$\pi^- p \to X$ [dashed line in Fig. 22(a)]. The agreement
between the distribution and the curve is striking.

Figure 22(c) shows $\langle n_X \rangle$ for resonant production
plus background as a function of $|t|$ and Fig. 22(d),
the equivalent data for the background sample.

TABLE III. Parameters obtained by fits of the indicated expressions to the $<n_X>$ data for
$\pi^- p \to p X$ at 147 GeV/c for $M_X^2 \geq 20$ GeV^2/c^4 and $|t| < 1.4$ GeV^2.

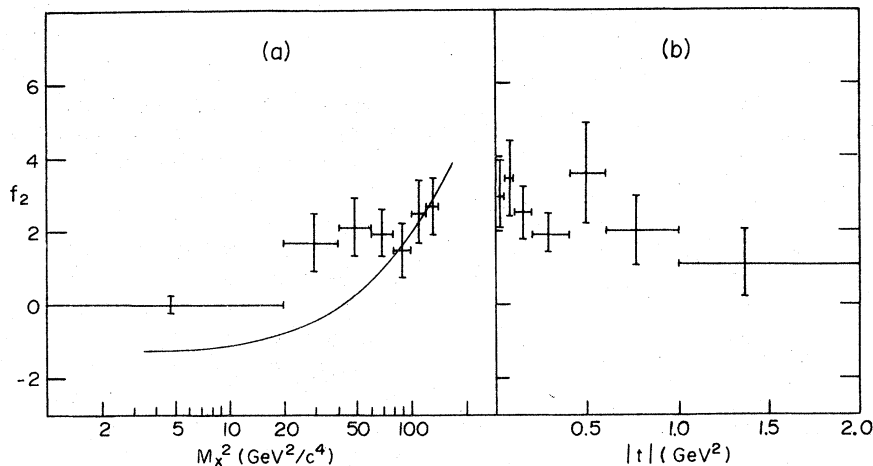| Expression	A	B	C	χ^2/ND
$A + B \ln M_X^2 + C|t|$	-0.87 ± 0.54	1.49 ± 0.14	0.64 ± 0.26	1.02
$A + B \ln M_X^2 + C (\ln M_X^2)^2$	7.46 ± 4.10	-2.74 ± 2.00	0.54 ± 0.24	0.71
$A + B M_X$	2.02 ± 0.25	0.43 ± 0.03		0.58
$A + B \ln(M_X^2/(1 + |t|))$	-1.58 ± 0.53	1.88 ± 0.14		2.71

FIG. 17. The Mueller parameter $f_2 = \langle n (n-1) \rangle - \langle n \rangle^2$ for $\pi^- p \to \pi^-_{fast} X$ at 147 GeV/c: (a) f_2 as a function of M_X^2. The solid line indicates the data for $\pi^- p \to X$ (Ref. 18); (b) f_2 as a function of $|t|$.

These data have been fit with the expressions $A + B \ln M_X^2$ and $A + C|t|$, and the resulting parameters are given in Table V. The solid lines in Fig. 22 are calculated from these fits. The fact that the results for the background sample are similar to those for the sample comprising resonant production plus background suggests that the same mechanism, π exchange, is responsible for both ρ production and the background, which is mainly s wave in this mass region.

D. $\pi^- p \to \Lambda^0 X$

The Λ^0 particles from the reaction $\pi^- p \to \Lambda^0 X$ are produced both in the target fragmentation and the central regions of rapidity.[30] However, as can be seen from the M_X^2 vs $|t|$ scatterplot given in Fig. 23, there is a strong correlation between the values of M_X^2 and $|t|$ except in the target fragmentation region ($|t| < 1$ GeV^2). The consequence of this, together with the small size of the sample,
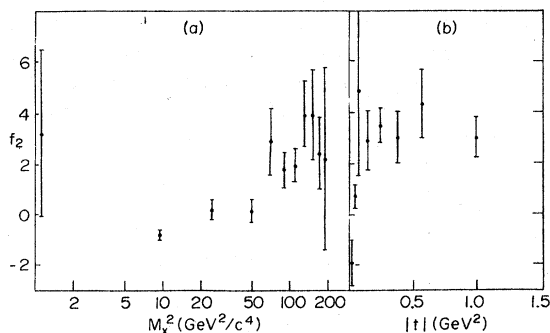
is that the results of fits of the expression $A + B \ln M_X^2 + C|t|$ to the $\langle n_x \rangle$ distributions over the whole range of both variables give results which are dependent on how the bins are chosen. Consequently, we have limited our analysis to Λ^0's produced in the hemisphere in the target direction and we

FIG. 18. The parameter $f_2 = \langle n (n-1) \rangle - \langle n \rangle^2$ for $\pi^- p \to p X$ at 147 GeV/c: (a) f_2 as a function of M_X^2; (b) f_2 as a function of $|t|$.
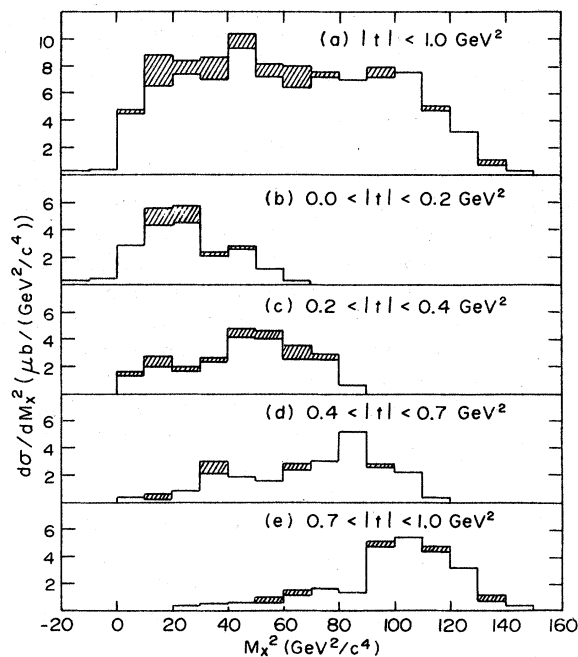

FIG. 19. The differential cross section, $d\sigma/dM_X^2$, as a function of M_X^2 in various regions of $|t|$, for $\pi^- p \to \Delta^{++} X$ at 147 GeV/c. The shaded areas represent events with four charged particles and no neutrals (i.e., events in which the data satisfied four constraint kinematic fits).
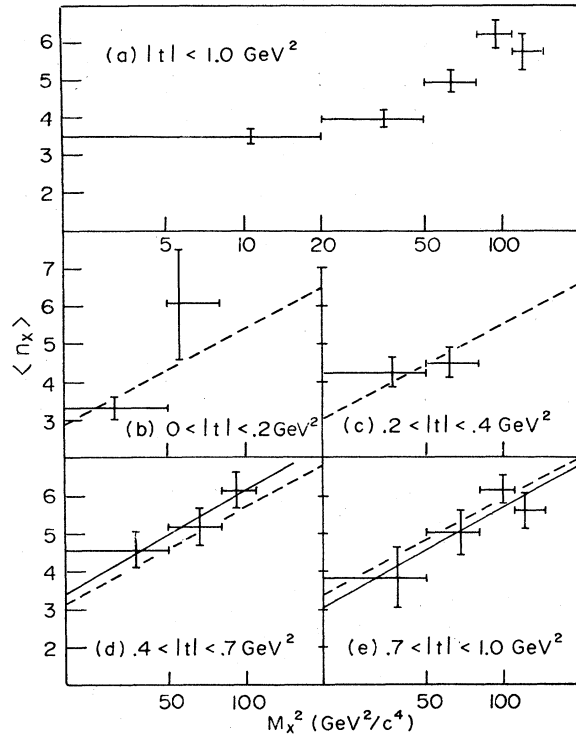
FIG. 20. The average charged-particle multiplicity $\langle n_X \rangle$ for $\pi^- p \to \Delta^{++} X$ at 147 GeV/c, as a function of M_X^2 in various regions of $|t|$. The solid lines give the results of fits of expression (19) to the data. The dashed lines give the results of two variable fits of expression (23) to the data, evaluated at the average values of $|t|$ in the given interval. The four-prong, four-constraint events are not included.

FIG. 21. The average charged-particle multiplicity, $\langle n_X \rangle$, for $\pi^- p \to \Delta^{++} X$ at 147 GeV/c, as a function of $|t|$ in various intervals of M_X^2. The solid lines give the results of fits of expression (21) to the data. The dashed lines give the results of two-variable fits of expression (23) to the data, evaluated at the average of M_X^2 in the given interval.

present results only for one-variable fits to the data for which the sample size is sufficient to provide bin independent results. Figure 24 gives the $\langle n_X \rangle$ distributions with respect to M_X^2 both for all events in the target hemisphere ($|t| < 14$ GeV^2) and for those in the target-fragmentation region ($|t| < 1$ GeV^2). The $\langle n_X \rangle$ distributions with respect to t are given for all events with $M_X^2 \geq 20$ GeV$^2/c^4$ and for those with $20 \leq M_X^2 \leq 140$ GeV$^2/c^4$. The parameters obtained in one-dimensional fits to these distributions are given in Table VI and the straight lines shown in Fig. 24 are calculated from these results. The values obtained for the
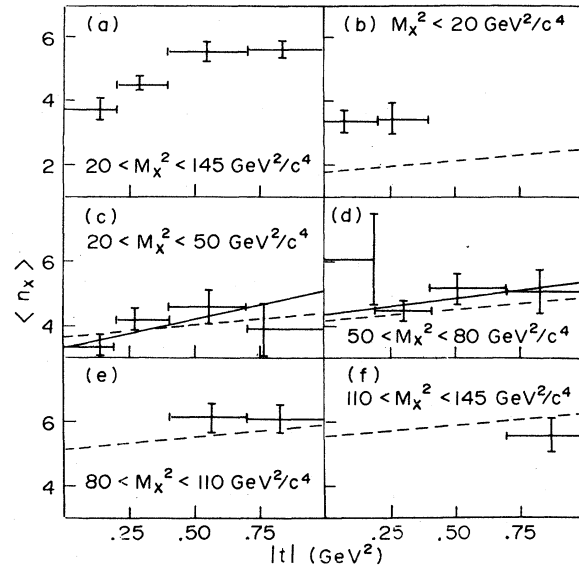
parameter B for the two t regions are found to be in good agreement. Those obtained for the parameter C agree within the uncertainties, but only that for $M_X^2 \geq 20$ GeV$^2/c^4$ is significantly greater than zero.

Data were also available for K^0 and $\bar{\Lambda}^0$ inclusive reactions, and both of these particle types were found to be produced only in the central region of rapidity.[30] This precluded a meaningful $\langle n_X \rangle$ analysis since the events corresponded to only a very narrow range of M_X^2.

V. DISCUSSION

Our results for $\pi^- p \to \pi_{\text{fast}}^- X$ and $\pi^- p \to p X$ are consistent with the assumption that $\langle n_X \rangle = A + B \ln M_X^2$ is a good representation of the M_X^2 dependence of $\langle n_X \rangle$ for $20 < M_X^2 < 140$ GeV$^2/c^4$ and that B is independent of reaction type. Although we

TABLE IV. Parameters obtained by fits of $A + B \ln M_X^2 + C|t|$ to $<n_X>$ data for $\pi^- p \to \Delta^{++} X$ at 147 GeV/c for $M_X^2 \geq 20$ GeV$^2/c^4$ and $|t| < 1.0$ GeV^2 with and without the four-prong four-constraint events ($\pi^- p \to \Delta^{++} \pi^- \pi^-$).

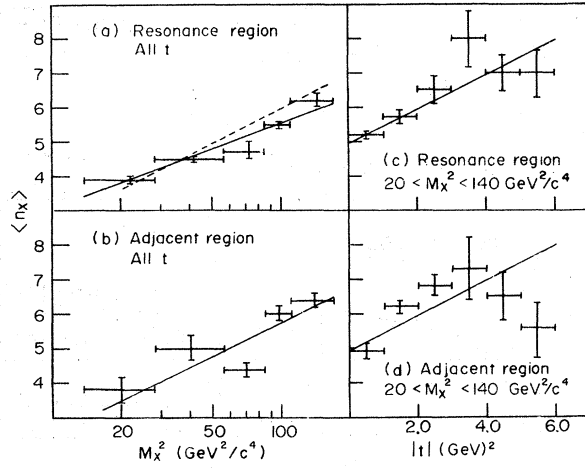|	A	B	C	χ^2/ND
Without	-1.89 ± 1.65	1.56 ± 0.49	0.72 ± 0.86	0.99
With	-2.01 ± 1.84	1.50 ± 0.54	0.94 ± 0.96	1.39

FIG. 22. The average charged multiplicity, $\langle n_X \rangle$, for $\pi^- p \to \pi^+ \pi^- X$ at 147 GeV/c for $\pi^+ \pi^-$ combinations with $x_{\pi^+\pi^-} \geq 0.5$. (a) Given as a function of M_X^2 for the ρ^0 region $(0.5 \leq M_{\pi^+\pi^-} \leq 1.0 \text{ GeV}/c^2)$ and (b) for the background regions $(0.26 \leq M_{\pi^+\pi^-} \leq 0.5 \text{ GeV}/c^2$ and $1.0 \leq M_{\pi^+\pi^-} \leq 1.4 \text{ GeV}/c^2)$. (c) Given as a function of $|t|$ for the ρ^0 region and (d) for the background region. The dashed curve in (a) gives the $\langle n_X \rangle$ vs s dependence for $\pi^- p \to X$ (see Table VIII). The solid curves give the results of fits of expression (19) to the data in (a) and (b), and expression (21) to the data in (c) and (d).

were not able to rule out other functional forms of the M_X^2 dependence for reactions (1)–(5) we will limit ourselves to this form in the subsequent discussion partially for phenomenological reasons and partially to permit inclusion of average total-inelastic charged-particle multiplicities which require this form.[14,17] The values of $\langle n_X \rangle$ at given M_X^2 are significantly different for reactions (1) and (2) and we therefore compared their $\langle n_X \rangle$ dependence on available energy, E_a. Figure 25, taken from our previous publication,[3] shows this comparison together with comparisons of $pp \to X$ (Ref. 18) and $\pi^- p \to X$ (Refs. 18, 36, 37) and of $\pi^- p \to pX$ (Ref. 8) and $pp \to pX$ (Ref. 20) at 205 GeV/c. Table VII gives the results of fitting these data with the expression
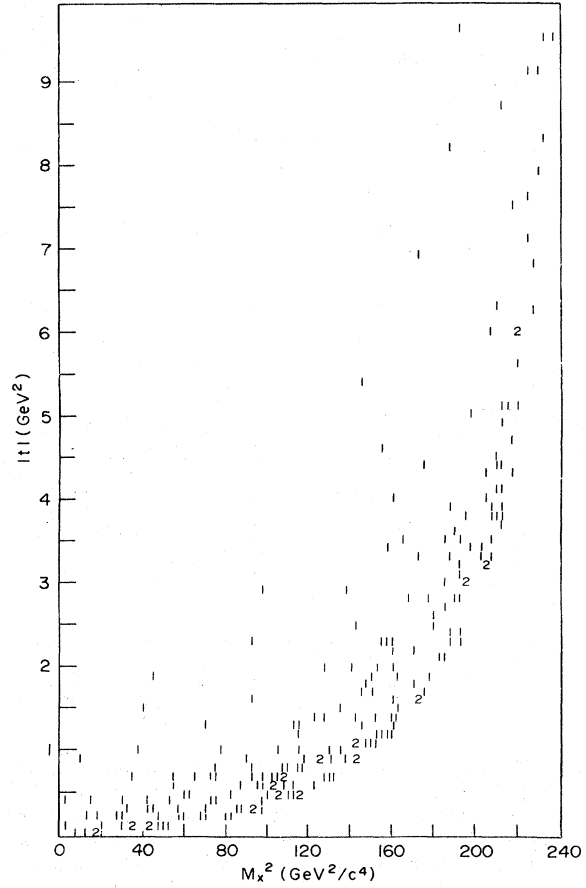

FIG. 23. The number of $\pi^- p \to \Lambda^0 X$ events at 147 GeV/c in each interval of M_X^2 and $|t|$.

$$\langle n_X \rangle = A' + B' \ln E_a^2 / E_{ao}^2 , \qquad (24)$$

where E_{ao} is the value of E_a at which one wishes to evaluate A'. By choosing E_{ao} in the center of the region for which data are available, one may avoid the large uncertainties that occur if A' is evaluated at $E_a = 1$, involving an extrapolation from the data region. Table VII also gives the

TABLE V. Parameters obtained by fits of the indicated expressions to $\langle n_X \rangle$ data for $\pi^- p \to (\pi^+ \pi^-) X$ at 147 GeV/c for $M_X^2 \geq 20$ GeV^2/c^4 and $x_{\pi^+ \pi^-} \geq 0.5$ in two $M_{\pi^+\pi^-}$ regions.

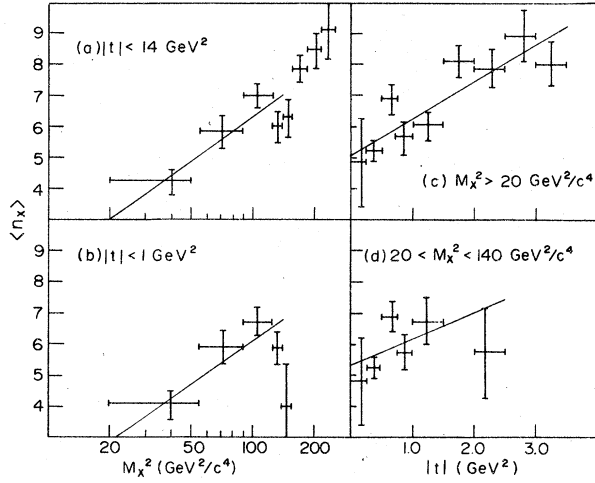| $M_{\pi^+\pi^-}$	Expression	A	B	C	χ^2/ND
$0.5 < M_{\pi^+\pi^-} < 1.0$ GeV/c^2	$A + B \ln M_X^2$	0.57 ± 0.33	1.08 ± 0.86		2.6
	$A + C|t|$	4.97 ± 0.12		0.49 ± 0.08	1.1
$0.26 < M_{\pi^+\pi^-} < 0.5$ GeV/c^2	$A + B \ln M_X^2$	-0.77 ± 0.82	1.41 ± 0.19		7.9
$1.0 < M_{\pi^+\pi^-} < 1.4$ GeV/c^2	$A + C|t|$	4.96 ± 0.17		0.50 ± 0.10	6.2

FIG. 24. The average charged multiplicity, $\langle n_X \rangle$, for $\pi^- p \to \Lambda^0 X$ at 147 GeV/c, as a function of M_X^2 for (a) $|t| < 14$ GeV^2 and (b) $|t| < 1$ GeV^2, and as a function of $|t|$ for (c) $M_X^2 \geq 20$ GeV^2/c^4 and (d) $20 \leq M_X^2 \leq 140$ GeV^2/c^4. The lines give the results of fits of expression (19) to the data in (a) and (b), and expression (21) to the data in (c) and (d).

FIG. 25. The average charged-particle multiplicity, $\langle n_X \rangle$, as a function of available energy, E_a, for (a) $\pi^- p \to X$ (Refs. 18, 36, 37) and $pp \to X$ (Ref. 18); (b) $\pi^- p \to pX$ and $pp \to pX$ at 205 GeV/c (Refs. 8 and 20, respectively), (c) $\pi^- p \to pX$ and $\pi^- p \to \pi_{\text{fast}}^- X$ at 147 GeV/c (this experiment). The solid lines are plotted from fits to the data of expression (24); the value E_{ao} in each plot is shown by the arrow.

difference $\delta A'$ between the results for A' for each pair of reactions. $\delta A'$ is the difference between the $\langle n_X \rangle$ values at the arrows for each pair of curves in Fig. 25. These differences are significant and display a systematic dependence on the particles involved.[3]

Therefore, we have analyzed our results in terms of a simple model which attempts to isolate the sources of these differences in $\langle n_X \rangle$. Figures 26(a) and 26(b) indicate schematically the approach that was taken. For inelastic hadron-hadron reactions $(a + b \to X)$, the average charged-particle multiplicity has contributions from both incoming particles, n_a and n_b, which depend on the particle type but not on s. There is also a contribution from the central region, n_0, which depends only on the extent of this region in rapidity and not on the nature of the incoming particles. In the simplest models this contribution is equal to a universal constant, the average number of particles per unit
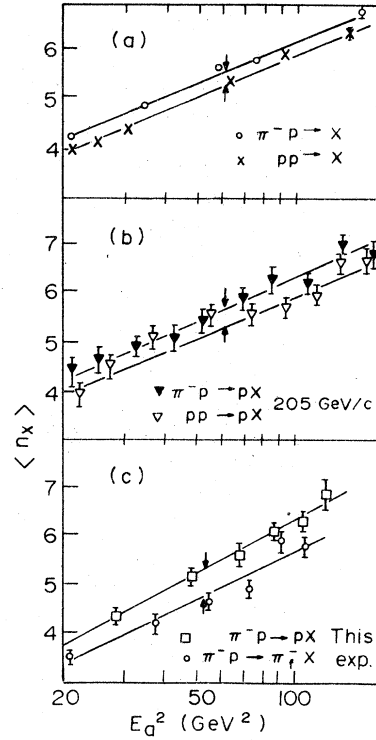
rapidity times the width in rapidity which is proportional to $\ln s$. Thus, for $a + b \to X$, this model predicts:

$$\langle n_X \rangle = n_a + B \ln s + n_b . \tag{25}$$

Analogously, for $a + b \to c + X$, there are contributions, n_0, from the central region which has a width proportional to $\ln M_X^2$ and, n_b, from particle b. However, in this inclusive reaction the exchanged particle or trajectory, E_{ac} [see Fig.

TABLE VI. Parameters obtained by fits of the indicated expression to $\langle n_X \rangle$ data for $\pi^- p \to \Lambda^0 X$ at 147 GeV/c.

Expression	Region fit	A	B	C	χ^2/ND
$A + B \ln M_X^2$	$|t| < 1.0$ GeV^2; $20 \leq M_X^2 \leq 140$ GeV^2/c^4	-3.10 ± 2.24	2.01 ± 0.52		2.0
	$|t| < 14$ GeV^2; $20 \leq M_X^2 \leq 140$ GeV^2/c^4	-3.14 ± 2.05	2.06 ± 0.47		2.8
$A + C|t|$	$20 \leq M_X^2 \leq 140$ GeV^2/c^4; $|t| < 3.5$ GeV^2	5.29 ± 0.45		0.87 ± 0.60	1.9
	$M_X^2 \geq 20$ GeV^2/c^4; $|t| < 3.5$ GeV^2	5.12 ± 0.31		1.17 ± 0.21	1.8

TABLE VII. Parameters obtained by fits of the expression $A' + B' \ln E_a^2/E_{a0}^2$ to $\langle n_X \rangle$ data for the six reactions of Fig. 25. E_{a0} is the central value of E_a in each pair of fits (see arrows in Fig. 25). Thus, A' is equal to the fitted value of $\langle n_X \rangle$ at E_{a0}. $\delta A'$ is the difference between the A' for each pair of reactions.

Reaction (X = anything)	E_{ao}	A'	B'	$\delta A'$	Data from Ref.
$\pi^-. + p \rightarrow X$		5.57 ± 0.04	1.25 ± 0.06		18, 36, 37
(i)	60 GeV			0.27 ± 0.06	
$p + p \rightarrow X$		5.30 ± 0.04	1.26 ± 0.05		18
$\pi^- + p \rightarrow p + X$		5.67 ± 0.06	1.30 ± 0.09		8
(ii) 205 GeV/c	60 GeV			0.30 ± 0.10	
$p + p \rightarrow p + X$		5.37 ± 0.08	1.23 ± 0.12		20
$\pi^- + p \rightarrow p + X$		5.28 ± 0.04	1.60 ± 0.07		this exp
(iii) 147 GeV/c	52 GeV			0.55 ± 0.12	
$\pi^- + p \rightarrow \pi_f^- + X$		4.73 ± 0.11	1.40 ± 0.17		this exp

26(b)] takes the place of incoming particle a in the total-inelastic reaction [see Fig. 26(a)]. This contributes $n_{E_{ac}}$ to the charged multiplicity, a contribution which might be expected to depend on both the nature of the exchange, its four-momentum transfer, t, and possibly the ratio s/M^2.
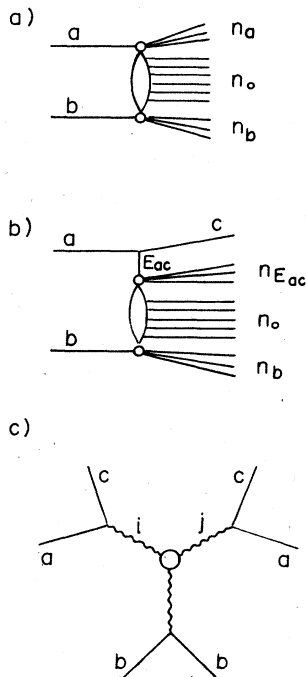

FIG. 26. (a) Diagram for reactions of the type $a + b \rightarrow X$, showing contributions to the total multiplicity from the projectile region, n_a, the target region, n_b, and the central region, n_0. (b) Diagram for reactions of the type $a + b \rightarrow c + X$, where the exchanged entity E_{ac} interacts with b to produce X. The multiplicity $\langle n_X \rangle$ has contributions $n_{E_{ac}}$, n_0, and n_b, analogous to those shown in (a). (c) Triple-Regge diagram for $a + b \rightarrow c + X$.

Thus, for $a + b \rightarrow c + X$, this model predicts

$$\langle n_X \rangle = n_{E_{ac}} + B \ln M_X^2 + n_b. \tag{26}$$

In particular, the coefficients B and n_b are the same as in Eq. (25). There is some arbitrariness in the separation of n_0 from the fragmentation regions which is reflected in the choice of scale for M_X^2 and s in the logarithm. However, comparisons between the coefficients are meaningful if the same scale is always used.

For various reasons a precisely linear dependence on $\ln M_X^2$ is not expected. For one, the fits of Albini *et al.*[14] to total-inelastic multiplicities for various incident particles show that $\langle n_X \rangle = A + B \ln s$ is a good representation of the data only over limited regions in s. Especially in the case of $pp \rightarrow X$, data are available over a large enough region of s that a simple linear dependence on $\ln s$ may be ruled out (see Fig. 1). This could be accommodated within the model by a quadratic dependence of n_0 on $\ln s$ or $\ln M_X^2$ which, like the linear dependence, is independent of the nature of the incident particle. It may also be accommodated in a Mueller-Regge analysis which takes into account a nonleading Regge trajectory.[13]

Another reason for not expecting a precisely linear dependence on $\ln M_X^2$ is that the term $n_{E_{ac}}$ may depend on s/M_X^2. The Mueller-Regge model predicts the dependence given by expressions (25) and (26), but states, in addition, that $n_{E_{ac}}$ is a scaling function of s/M_X^2.[38] To the extent that one trajectory predominates at high s/M_X^2, it is expected that $n_{E_{ac}}$ would be essentially independent of s/M_X^2 and dependent on t only. However, an explicit dependence upon s/M_X^2 at low values of this parameter would produce a departure in $\langle n_X \rangle$ from the linear form $A + B \ln M_X^2$ for a fixed s.

TABLE VIII. Parameters obtained by fits of the expressions $A'' + B \ln M_X^2/53$ or $A'' + B \ln s/53$ to $\langle n_X \rangle$ data for various reactions for $20 < M_X^2 < 140$ GeV$^2/c^4$ or $20 < s < 140$ GeV^2.

Reaction	Momentum (GeV/c)	Reference	No. points	A''	B	χ^2/ND
$\pi^- p \to \pi_f^- X$	147	this exp	6	4.35 ± 0.08	1.65 ± 0.15	1.8
$\pi^- p \to p X$	147	this exp	6	5.28 ± 0.08	1.63 ± 0.14	0.5
	205	39	9	5.34 ± 0.08	1.21 ± 0.14	0.4
$\pi^- p \to \pi^- p X$	147	this exp	3	5.81 ± 0.35	1.73 ± 0.68	0.3
$\pi^- p \to \Delta^{++} X$	147	this exp	4	4.70 ± 0.15	1.83 ± 0.32	1.3
$\pi^- p \to (\pi^+ \pi^-)_{\rho 0} X$	147	this exp	5	4.85 ± 0.06	1.08 ± 0.09	2.6
$\pi^- p \to \Lambda^0 X$	147	this exp	4	4.97 ± 0.28	1.82 ± 0.45	3.0
$\pi^+ p \to \Delta^{++} X$	100	40	4	4.98 ± 0.25	0.84 ± 0.58	0.4
$\pi^+ p \to \Lambda^0 X$	100	41	3	5.94 ± 0.65	1.27 ± 0.95	0.2
$pp \to p X$	102	7	7	4.54 ± 0.11	0.96 ± 0.17	0.8
	205	20	9	4.75 ± 0.06	1.24 ± 0.10	1.4
	303	6	7	5.57 ± 0.18	1.11 ± 0.31	1.3
	400	7	3	4.86 ± 0.24	2.03 ± 0.51	0.03
$pp \to \Delta^{++} X$	100	40	6	4.61 ± 0.23	0.53 ± 0.47	2.6
	102	42	3	4.32 ± 0.27	1.61 ± 0.54	2.2
	205	43	5	4.22 ± 0.07	1.17 ± 0.13	0.8
	400	42	3	3.52 ± 0.40	0.83 ± 0.64	0.3
$pp \to \Lambda^0 X$	100	41	5	4.91 ± 0.44	1.69 ± 0.69	0.5
$pp \to X$		14, 44, 45	19	4.48 ± 0.01	1.38 ± 0.03	1.7
$\bar{p} p \to X$		14	4	4.87 ± 0.05	1.23 ± 0.12	1.1
$\pi^+ p \to X$		14, 18, 44, 45	9	5.13 ± 0.03	1.21 ± 0.05	5.0
$\pi^- p \to X$		14, 18	12	5.03 ± 0.02	1.45 ± 0.03	2.2
$K^+ p \to X$		14, 18, 45	5	4.86 ± 0.03	1.30 ± 0.05	1.4
$K^- p \to X$		14	5	4.74 ± 0.03	1.38 ± 0.05	2.2

In Table VIII we give the results of a fit of

$$\langle n_X \rangle = A'' + B \ln M_X^2/53 \qquad (27)$$

to our data for reactions (1) to (5) for $20 \leqslant M_X^2 \leqslant 140$ GeV$^2/c^4$. In this table we also present the results of fits of (27) to data for inclusive reactions from the literature and of

$$\langle n_X \rangle = A'' + B \ln s/53 \qquad (28)$$

to various inelastic processes for the same region of M_X^2 or s as our data. It should be noted that the inclusive $\langle n_X \rangle$ can be fit by other functions of M_X and substantially higher statistics would be required to permit a unique decision on functional form. However, the total inelastic $\langle n_X \rangle$ require an $\ln s$ dependence,[14,17] and therefore we have chosen this form in order to simultaneously describe all the reactions in Table VIII over the given range in M_X^2 and s. All the values of B agree within three standard deviations with the weighted average value, 1.35 ± 0.09. All the $X^2/$ND are acceptable except that for $\pi^+ p \to X$. The values of B for $pp \to X$ and $\bar{p} p \to X$ are consistent with those obtained by Albini *et al.*[14] for somewhat different regions of s.

Since data are available for some of the inclusive reactions at several values of incoming beam momentum, it is possible to investigate the dependence of the term, $n_{E_{ac}}$, on s/M_X^2. This exchange contribution is given by the following expressions for $\pi^- p \to pX$ and $pp \to pX$, respectively,

$$n_{E_{pp}} = \langle n_X \rangle - n_0 - n_{\pi^-}, \qquad (29)$$

$$n_{E_{pp}} = \langle n_X \rangle - n_0 - n_p. \qquad (30)$$

The n_0 term may be assumed to be $B \ln M_X^2$ where B is the slope obtained for the particular reaction given in Table VIII. This choice, however, suffers from the difficulty that all the M_X^2 dependence in these fits is lumped in this term. A less biased approach is to use the values obtained for B in the fits to total-inelastic $\langle n_X \rangle$ reactions (8)–(13), the weighted average of which is 1.35. n_{π^-} and n_p are not known, but their difference may be obtained from $pp \to X$ and $\pi^- p \to X$ and is given in Table IX. Thus, the same quantity, $n_{E_{pp}} + n_p$, in this model may be plotted for both reactions. For $\pi^- p \to pX$, this quantity is equal to the following:

$$n_{E_{pp}} + n_p = \langle n_X \rangle - n_0 - (n_\pi - n_p)$$
$$= \langle n_X \rangle - 1.35 \ln M_X^2 - 0.55 \qquad (31)$$

and for $pp \to pX$,

$$n_{E_{pp}} + n_p = \langle n_X \rangle - n_0 = \langle n_X \rangle - 1.35 \ln M_X^2. \qquad (32)$$

TABLE IX. Terms in the expressions $\langle n_X \rangle = n_{E_{ac}} + B \ln M_X^2 + n_b$ and $\langle n_X \rangle = n_a + B \ln s + n_b$ calculated from the results given in Table VIII (see text for explanation).

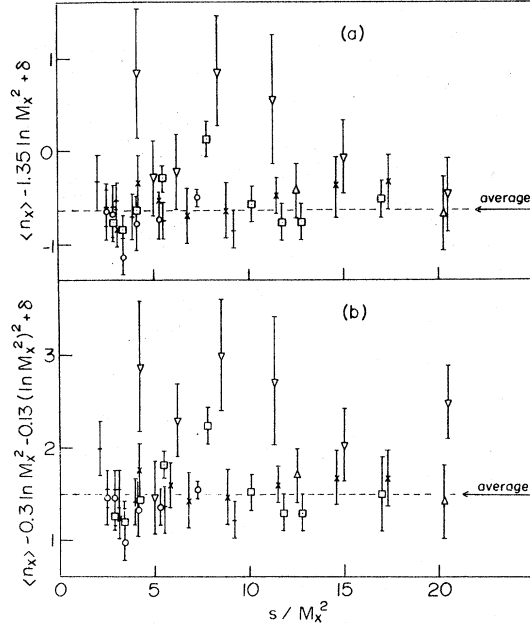| Term	Momentum (GeV/c)	Result	Weighted average
$n_{\pi^+} - n_{\pi^-} = A''\ (\pi^+ p \to X) - A''\ (\pi^- p \to X)$		0.09 ± 0.03	
$n_{K^+} - n_{K^-} = A''\ (K^+ p \to X) - A''\ (K^- p \to X)$		0.12 ± 0.04	
$n_p - n_{\bar{p}} = A''\ (pp \to X) - A''\ (\bar{p}p \to X)$		-0.39 ± 0.05	
$n_{\pi^+} - n_p = A''\ (\pi^+ p \to X) - A''\ (pp \to X)$		0.64 ± 0.03	
$A''\ (\pi^+ p \to \Delta^{++} X) - A''\ (pp \to \Delta^{++} X)$	100	0.37 ± 0.36	0.64 ± 0.03
$A''\ (\pi^+ p \to \Lambda^0 X) - A''\ (pp \to \Lambda^0 X)$	100	1.03 ± 0.78	
$n_{\pi^-} - n_p = A''\ (\pi^- p \to X) - A''\ (pp \to X)$		0.55 ± 0.03	0.55 ± 0.03
$A''\ (\pi^- p \to p X) - A''\ (pp \to p X)$	205	0.59 ± 0.10	
$n_{\pi^-} - n_{K^-} = A''\ (\pi^- p \to X) - A''\ (K^- p \to X)$		0.29 ± 0.04	
$n_{E_{pp}} - n_{E_p \Delta^{++}} = A''\ (pp \to p X) - A''\ (pp \to \Delta^{++} X)$	102	0.22 ± 0.29	
$A''\ (\pi^- p \to p X) - A''\ (\pi^- p \to \Delta^{++} X)$	147	0.57 ± 0.17	0.54 ± 0.08
$A''\ (pp \to p X) - A''\ (pp \to \Delta^{++} X)$	205	0.52 ± 0.09	
	400	1.35 ± 0.47	
$n_{E_{pp}} - n_{E_p \Lambda} = A''\ (pp \to p X) - A''\ (pp \to \Lambda^0 X)$	102, 100	-0.36 ± 0.45	0.09 ± 0.26
$A''\ (\pi^- p \to p X) - A''\ (\pi^- p \to \Lambda^0 X)$	147	0.31 ± 0.31	
$n_{E_{pp}} - n_p = A''\ (pp \to p X) - A''\ (pp \to X)$	102	0.06 ± 0.11	
$A''\ (\pi^- p \to p X) - A''\ (\pi^- p \to X)$	147	0.24 ± 0.08	
$A''\ (\pi^- p \to p X) - A''\ (\pi^- p \to X)$	205	0.30 ± 0.09	0.28 ± 0.04
$A''\ (pp \to p X) - A''\ (pp \to X)$	205	0.26 ± 0.06	
	303	1.08 ± 0.18	
	400	0.38 ± 0.24	
$n_{E_{\pi^- \pi^-}} - n_{\pi^-} = A''\ (\pi^- p \to \pi_f^- X) - A''\ (\pi^- p \to X)$	147	-0.68 ± 0.09	
$n_{E_{\pi^-(\pi^+\pi^-)_{\rho 0}}} - n_{\pi^-} = A''(\pi^- p \to (\pi^+\pi^-)_{\rho 0} X) - A''(\pi^- p \to X)$	147	0.18 ± 0.07	

FIG. 27. (a) The quantity $\langle n_X \rangle - 1.35 \ln M_X^2 + \delta$ plotted as a function of s/M_X^2 for $pp \to pX (\delta = 0)$ at 102 GeV/c ($\odot$), 205 GeV/c ($\boxdot$), 303 GeV/c ($\triangledown$), and 400 GeV/c ($\triangle$), and $\pi^- p \to pX$ ($\delta = -0.55$) at 147 GeV/c ($\times$) and 205 GeV/c ($+$). This quantity is equivalent to $n_{E_{pp}}(s/M_X^2, \langle t \rangle) + n_p$ according to the model discussed in the text, if $n_0 = 1.35 \ln M_X^2$; (b) the quantity $\langle n_X \rangle - 0.31 \ln M_X^2 - 0.13\ (\ln M_X^2)^2$ plotted as a function of s/M_X^2 for the same reactions. This quantity is equivalent to $n_{E_{pp}}(s/M_X^2, \langle t \rangle) + n_p$ if $n_0 = 0.31 \ln M_X^2 + 0.13\ (\ln M_X^2)^2$.

These expressions from the two reactions are given as a function of s/M_X^2 in Fig. 27(a) and are seen to be consistent with a constant value of -0.63 ± 0.03 ($\chi^2/\text{ND} = 2.0$). It should be pointed out
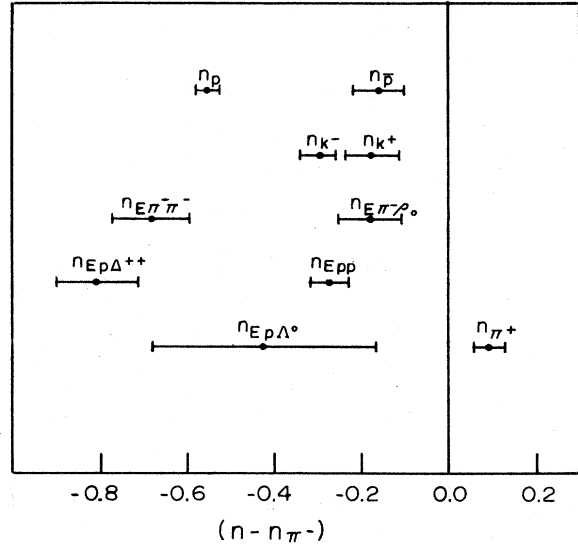

FIG. 28. The difference between the multiplicity associated with a specific particle or exchanged entity and that associated with the π^- (n_{π^-}), as determined from combinations of reactions listed in Table VIII for s or $M_X^2 = 53$ GeV$^2/c^4$.

that the $\langle n_X \rangle$ at different s and M_X^2 values correspond to data extending over different intervals in t. Since $n_{E_{pp}}$ is expected to be a function of t, this could affect the results in Fig. 27. However, as discussed in the previous section, the t dependence of $\langle n_X \rangle$ in those inclusive reactions where it has been measured is not strong and, consequently, a significant effect is not expected.

To test whether the apparent constancy of $n_{E_{pp}}$ is due to the assumption of a linear dependence upon $\ln M_X^2$, we also tried the expression $n_0 = 0.30 \ln M_X^2 + 0.13 (\ln M_X^2)^2$, the fit to the data for $pp \to X$ obtained by Albini *et al.*[14] (see Fig. 1). The results shown in Fig. 27(b) are consistent with a constant value $n_{E_{pp}} + n_p = 1.50 \pm 0.04$ ($\chi^2/\text{ND} = 1.8$). The difference in the absolute value from the result obtained above is due to the different convention for defining n_0 and is unimportant. The results of both calculations indicate that a function which approximates the s dependence of total-inelastic charged multiplicities also accounts for the M_X^2 dependence of the inclusive charged multiplicities within the uncertainties. Thus, over the region covered, $n_{E_{pp}}$ does not have a significant s/M_X^2 dependence.

The values for $\langle n_X \rangle$ at M_X^2 equal to 53 GeV^2/c^4 given in Table VIII make it possible to calculate the difference between various contributions to the charged-particle multiplicities by subtracting $\langle n_X \rangle$ for the appropriate reactions. For example, since for $\pi^+ p \to X$, $(\langle n_X \rangle)_{\pi^+ p} = n_{\pi^+} + n_0 + n_p$, and for $\pi^- p \to X$, $(\langle n_X \rangle)_{\pi^- p} = n_{\pi^-} + n_0 + n_p$, it follows that $(\langle n_X \rangle)_{\pi^+ p} - (\langle n_X \rangle)_{\pi^- p} = n_{\pi^+} - n_{\pi^-}$. This result is independent of the functional form of the M_X^2, but does assume that it is the same for all reactions. Table IX gives the results for a number of such differences and in the seventeen cases where the same term difference corresponds to more than one difference between reactions, the results agree with the weighted average value within the uncertainties. From the values in Table IX, it is possible to calculate relative values for most of the terms. Choosing $n_{\pi^-} = 0$, one obtains the values given in Fig. 28. The relative values of these parameters are shifted, but not by more than 2 standard deviations if one evaluates the differences at $M_X^2 = 106$ GeV^2/c^4, using the values of B obtained by the fits to the individual reactions. However, the pattern is the same.

It is interesting to see if the contributions $n_{E_{ab}}$ have the characteristics to be expected from the exchange of a virtual particle of the appropriate quantum number. Since a π^--like exchange occurs in the process $\pi^- \to \rho^0$ one might expect that $n_{\pi^-} \sim n_{E_{\pi - \rho 0}}$, and, indeed, we see in Fig. 28 that this is true. Furthermore, since a K^+-like exchange occurs in the process $p \to \Lambda$, we expect

that $n_{K^+} \sim n_{E_{p\Lambda}}$, which again is observed. However, although the process $p \to \Delta^{++}$ has been observed to proceed predominantly by π^- exchange at 147 GeV/c,[28] the $n_{E_{p\Delta^{++}}}$ term obtained from these data is significantly different from n_{π^-}. It agrees with $n_{E_{\pi - \pi -}}$, which could be explained by ρ exchange being important in both processes. This is in agreement with the results of a triple-Regge analysis of this reaction at 15 GeV/c which show that the exchange to the $p\Delta^{++}$ vertex lies between the π and ρ trajectories.[46]

VI. SUMMARY AND CONCLUSIONS

We have described the analysis of and some of the results for reactions (1) to (5) at 147 GeV/c. For all of these reactions, the inclusive average charged multiplicity was consistent with a linear dependence on $\ln M_X^2$, but other functional forms could also be fit to the data. $\langle n_X \rangle$ for $\pi^- p \to \pi^-_{\text{fast}} X$ had a significant t dependence, and the t dependence found for $\pi^- p \to p X$ was nonzero by more than 2 standard deviations. A comparison of the data for $\pi^- p \to \rho^0 X$ with those for $\pi^- p \to X$ indicates that the average charged multiplicity for off-mass-shell "π" p scattering is very similar to that for on-mass-shell πp scattering.

Our analysis has shown that the average charged multiplicities are not described by a universal function of available energy. Thus, we have compared our data and data from the literature with a simple model which gives $\langle n_X \rangle$ as the sum of one term from each of the incoming particles, one of which is the exchanged particle in the case of inclusive reactions, and a universal term from the central region which is a function of s or M_X^2. Other studies have shown that over a limited region in s, $B \ln s$ is in satisfactory agreement with the observed s dependence of the experimental results, but a quadratic term is needed for $pp \to X$ over a wider region.[14,17] The values obtained in this study for B are consistent with the average value, 1.35 ± 0.09, for all reactions considered. In inclusive reactions, the contribution from the exchanged particle, $n_{E_{ab}}$, would be expected to be a function of s/M_X^2 and t. A significant t dependence is observed in $\pi^- p \to \pi^-_{\text{fast}} X$, but no evidence for an s/M_X^2 dependence was found.

We have calculated differences between various contributions to the average multiplicities by taking the difference between average multiplicities at M_X^2 or $s = 53$ GeV^2 for different reasons. This has enabled us to establish the relative magnitudes of the terms contributing to the multiplicities as given in Fig. 28. Since a number of the term differences are calculated from differences between more than one pair of reactions,

the consistency of these results constitutes a consistency check on the model.

ACKNOWLEDGMENTS

*Present address: DESY, Hamburg, West Germany.

†Present address: New England Nuclear, Billerica, Massachusetts.

‡Present address: Polytechnic Institute of New York, Brooklyn, New York.

§Present address: Indiana University, Bloomington, Indiana.

‖Present address: Purdue University, West Lafayette, Indiana.

¶Present address: Argonne National Laboratory, Argonne, Illinois.

**Present address: Dialog Systems, Inc., Belmont, Massachusetts.

††Present address: Duke University, Durham, North Carolina.

‡‡On leave of absence from Tel-Aviv University, Tel-Aviv, Israel.

§§Present address: Stanford Linear Accelerator Center, Stanford, California.

‖‖Present address: Tel-Aviv University, Tel-Aviv, Israel.

¶¶Present address: The Weizmann Institute of Science, Rehovot, Israel.

***Present address: Fermilab, Batavia, Illinois.

[1]D. Fong et al., Phys. Lett. 53B, 290 (1974).

[2]D. Fong et al., Nucl. Phys. B102, 386 (1976).

[3]Proportional Hybrid System Consortium, Phys. Rev. Lett. 37, 736 (1976).

[4]W. R. Frazer and D. R. Snider, Phys. Lett. 45B, 136 (1973).

[5]C. F. Chan, Phys. Rev. D 8, 179 (1973).

[6]S. J. Barish et al., Phys. Rev. Lett. 31, 1080 (1973).

[7]J. P. DeBrion et al., Phys. Lett. 52B, 477 (1974).

[8]F. C. Winkelmann et al., Phys. Rev. Lett. 32, 121 (1974).

[9]C. F. Chan and F. C. Winkelmann, Phys. Rev. D 10, 3645 (1974).

[10]W. R. Frazer et al., Rev. Mod. Phys. 44, 284 (1972).

[11]E. L. Feinberg, Phys. Rep. 5C, 240 (1972).

[12]M. Garetto et al., Nuovo Cimento 38, 38 (1977).

[13]D. M. Tow, Phys. Rev. D 7, 3535 (1973).

[14]E. Albini et al., Nuovo Cimento 32, 101 (1976).

[15]J. Whitmore, Phys. Rep. 10C, 273 (1974).

[16]J. Whitmore, Phys. Rep. 27C, 187 (1976).

[17]W. Thome et al., Nucl. Phys. B129, 365 (1977).

[18]V. V. Ammosov et al., Nucl. Phys. B58, 77 (1973).

[19]A. Wroblewski, High Energy Physics, proceedings of the Fifteenth International Conference on High Energy Physics, Kiev, 1970, edited by V. Shelest (Naukova Dumka, Kiev, U.S.S.R., 1972), p. 42.

[20]J. Whitmore and M. Derrick, Phys. Lett. 50B, 280 (1974).

[21]C. Pajares and R. Pascual, Nucl. Phys. B137, 390 (1978).

[22]M. G. Albrow et al., Nucl. Phys. B102, 275 (1976).

[23]J. W. Chapman et al., Phys. Rev. Lett. 36, 124 (1976) (this paper includes references to previous work); D. Horn, rapporteur talk, Oxford Conference on Multiparticle Production, 1975 (unpublished).

[24]S. J. Brodsky and J. F. Gunion, Phys. Rev. Lett. 37, 402 (1976).

[25]A. Casher, J. Kogut, and L. Susskind, Phys. Rev. Lett. 31, 792 (1978).

[26]The topology dependent weights, w_i, are given by $w_i = \sigma_i/N_i$ where σ_i is the cross section for the i prong topology and N_i is the number of usable events in that topology.

[27]Here, as usual, $x = 2p_L^*/\sqrt{s}$ where p_L^* is the longitudinal momentum of the particle in the center-of-mass system and $\sqrt{s}$ is the center-of-mass energy.

[28]D. Brick et al., Phys. Rev. D 18, 3099 (1978).

[29]D. Fong et al., Phys. Lett. 60B, 124 (1975).

[30]Proportional Hybrid System Consortium, report (unpublished).

[31]See, for example, J. Bartsch et al., Phys. Lett. 27B, 336 (1968).

[32]Particle Data Group, Phys. Lett. 50B, 1 (1974).

[33]$f_2 = \langle n(n-1) \rangle - \langle n \rangle^2$.

[34]J. Whitmore et al., Phys. Rev. D 11, 3124 (1975).

[35]F. Barreiro et al., Phys. Rev. Lett. 40, 595 (1978).

[36]G. A. Akopdjanos et al., Nucl. Phys. B75, 401 (1974).

[37]E. L. Berger et al., Nucl. Phys. B77, 365 (1974).

[38]C. E. DeTar, Phys. Rev. D 17, 870 (1978).

[39]F. C. Winkelmann et al., Phys. Lett. 48B, 273 (1974).

[40]J. Erwin et al., Phys. Rev. Lett. 35, 980 (1975).

[41]J. Erwin et al., Phys. Rev. D 16, 553 (1977).

[42]J. P. DeBrion et al., Phys. Rev. Lett. 34, 910 (1975).

[43]S. J. Barish et al., Phys. Rev. D 12, 1260 (1975).

[44]C. Bromberg et al., Phys. Rev. D 15, 64 (1977).

[45]W. W. Morse et al., Phys. Rev. D 15, 66 (1977).

[46]F. Barreiro et al., Phys. Rev. D 17, 681 (1978).